QATAR UNIVERSITY

COLLEGE OF ENGINEERING

# FAULT DETECTION AND LOCALIZATION IN MODULAR MULTILEVEL CONVERTER

BY

MAHDI HOUCHATI

A Thesis Submitted to

the Faculty of the College of

Engineering

in Partial Fulfillment

of the Requirements

for the Degree of

Masters of Science in Electrical Engineering

June 2018

# COMMITTEE PAGE

The members of the Committee approve the Thesis of Mahdi Houchati defended on 07/05/2018.

_____

Prof.
Lazhar Ben-Brahim
Thesis/Dissertation Supervisor

_____

Prof.
Adel Gastli
Thesis/Dissertation Supervisor

_____

[Dr.]
Mustafa Serkan Kiranyaz
Committee Member

_____

[Dr.]
S M Muyeen
Committee Member

_____

[Dr.]
Hisham Eid

Committee Member

Approved:

_____

Khalifa Al-Khalifa, Dean, College of Engineering

# ABSTRACT

HOUCHATI MAHDI, Masters : June : 2018, Masters of Science in Electrical Engineering

Title: Fault Detection and Localization in Modular Multilevel Converter

efficiently Supervisors of Thesis: Lazhar Ben Brahim, Adel Gastli.

The Modular Multilevel Converter is gaining wide acceptance in both industrial and research communities for medium and high power applications. However, the increasing need for a higher number of active power switches raised more reliability issues. In this study, detection and localization of open circuit faults are studied in depth. Two multivariate statistical techniques, namely the principal component analysis and the kernel principal component analysis are proposed for fault detection and localization. To study the effectiveness of the proposed methodologies, two converters with different sizes and control techniques are considered in the simulations. The results show that both techniques are capable of accurately detecting the anomalies that can disrupt the normal behavior of the converter. However, only the kernel principal component analysis, can efficiently localize the faulty cells.

# ACKNOWLEDGMENTS

I would like to express my sincere gratitude to my supervisors Prof. Lazhar Ben-Brahim and Prof. Adel Gastli for their continuous and endless support and patience during my Master thesis. Their comments and advice were very precious and inspiring. I would also like to seize this opportunity to express a special thanks to Dr. Nader Meskin for the provided help and support. I am very grateful for his valuable guidance and advice. Many thanks for sacrificing their times and conveying their knowledge to contribute to my learning and success. Additionally, I would like to extend my gratitude to all the electrical engineering department faculty, and staff members for the supportive, encouraging and friendly environment.

# TABLE OF CONTENTS

# LIST OF TABLES

# LIST OF FIGURES

# CHAPTER 1: INTRODUCTION

## 1.1 Background

"Everything that has a beginning has an end." A very famous quote, which implies that all systems can malfunction and fail. A 'fault' is an error or a problem that drives the system outside its intended work boundaries. This problem can lead to total failure or unwanted behavior of the system so that an immediate intervention should be compelled to restore the normal working conditions. Faults can affect the actuators, sensors or the plant component, and the severity of the fault impact ranges from partial failure to total failure of the system. Failures are inevitable if the system in hand is real and under real environment stress. As simplicity is vital for reliability, the more complex the system is, the more reliability flags are raised. However, due to the increasing needs of our daily life, most of the technological systems nowadays are complex. This increasing need to render the systems more complex urged the scientific and industrial worlds to study faults and implement techniques that would prevent them, or at least to remediate their effect and rejoin the normal behavior of the system at the earliest, to avoid economic losses, environmental impacts, and even life hazards. Subsequently, this has led to the appearance of the fault detection and isolation area that is a subfield of control engineering and is concerned with the monitoring of the system behavior to detect abnormalities and identify their locations. Among the variety of applications of fault detection and diagnosis, electrical systems can be considered as one of the most interesting areas of application since electrical systems can be critical and their failures can cause devastating impacts.

Power electronic devices are considered as the backbone of several electrical applications. However, despite their great development since their invention in 1957 and the amount of research done to enhance their performance, they still present many reliability challenges. Due to their advances, power electronic applications have been integrated into a great variety of fields such as renewable energy, generation, transmission and distribution of power energy and even automotive and aerospace industries that brought more strict reliability constraints. The vulnerability of power electronic devices was tested in several field studies. For instance, a study conducted on photovoltaic generating plant revealed that inverters were responsible for 37% of the unscheduled maintenance events and had a share of 59% of the unscheduled maintenance costs [1]. Another study that used the reports from multiple manufacturers to identify the failure sources in wind turbines showed that the converters were responsible for 13% of overall failure rate and had a share of 18.4% of overall downtime[2]. Examples of the impact of power electronic failures can also be found in [3],[4],[5]. Therefore, even if the initial cost of the power electronic devices may not be high, the impact of their failure on the system and downtimes that they engender can increase the overall cost drastically. According to Wolfgang E.'s work that was cited in [6], there are two major failure causes for power electronic systems depending on application and design; the capacitors and the semiconductors with failure risk shares of 30% and 21% respectively. A questionnaire was carried out about the industrial power electronic converters reliability and concluded that the most fragile components are the power switches [7]. These studies pinpoint the importance of studying the failure of the power electronic devices and more specifically the failures in power switches. In this regard, the lifetime of a particular device can be

divided using the bathtub curve into three regions where the first period is characterized by high fault probability that decreases overtime to reach the second period, which represents the useful life of the device with constant failure risk that is mostly related to random failures and working conditions. Finally, during the last period, the device is subjected to wear out and aging factors, which increase the failure probability. The useful lifetime of the device can be reduced according to its working and overstress conditions. Stresses on electronic devices can be classified into four major sources, namely, steady state and cyclical temperature with a share of 55%, vibration and shock with a share of 20%, humidity and moisture with a share of 19% and contaminants & dust with a share of 6% [8]. Before proceeding to fault detection techniques, it is worth mentioning the types of faults and the mechanism of failures in power switches. To begin with, faults in general can be manifested in different forms; for instance they can be abrupt, incipient or intermittent [9]. The abrupt failure is a sudden failure that occurs and does not clear without outside interference whilst the incipient failure continues to build up over time and finally the intermittent failure occurs at irregular intervals. The failure mechanism differs between different power switches based on their physical properties. However, since the Insulated-Gate Bipolar Transistor (IGBT) is the most used power switch in industrial applications[8], many researchers focused on the failure types and mechanisms of this particular model [10]–[15]. In fact, the power switch faults can be classified into two main categories, namely, the open circuit and the short circuit faults. Each of these two failures has its own failure mechanism and impact to other power devices and to the system in general. The root cause of failures in IGBTs can be a wear out or a catastrophic failure. Wear out is due to aging and degradation of the device over time. It includes bond wire lift-off, solder joint

fatigue, bond wire heel cracking, aluminum reconstruction, substrate cracking, interconnection corrosion, etc. All these factors are related to the durability of the device. The condition monitoring can be effective to identify abnormalities in the behavior of the system, and scheduled maintenance can help in preventing breakdowns and failures because of wear out. The catastrophic failures, on the other hand, happen suddenly and are mostly unpredictable. They can engender serious damage to the converter and to the overall system. According to [15], two failure mechanisms are related to open circuit failures, namely, the bond wire lift-off or rupture, which can be caused by a very high current, and external reasons such as disconnection caused by vibrations. Besides the absence of gate drive signals can lead to open circuit behavior in the system. As per the short circuit failures, four reasons can be accounted responsible based on the state of the IGBT, namely, the energy shocks caused by high power dissipation in short time during the on-state, the latch-up failures in which the collector current cannot be controlled by the gate signal, the second breakdown, which is caused by high current stress that stimulates local thermal breakdown, and the high voltage breakdown caused by the spikes of the voltage during turn-off. It should be mentioned that open circuit faults do not represent an immediate threat to the converter whereas the short circuit faults launch a chain reaction that can end up by causing the total failure of the system and fatal failures of other components [16]. Experts have always seen that dealing with short circuit faults is more challenging, since the IGBT cannot withstand the energy passing through for more than $10\mu s$, consequently limiting the software based methods that may detect the fault but cannot take actions towards its removal within the time limit. Therefore, hardware techniques are more suitable

for detection and isolation of a short circuit fault. On the other hand, the open circuit fault, which imposes less restraint conditions, can be dealt with using algorithm-based methods without requiring additional hardware implementation. Open circuit faults induce a DC current offset that create uneven stresses on the switches, thus affecting the performance of the system and may generate more faults.

## 1.2 Problem Statement

Since the power switches are always susceptible to fail because of wear out and random faults, under given working conditions, fault detection and localization are crucial for preserving the integrity of the system. The choice of the optimal solution for fault detection and localization depends on the complexity and efficiency of the detection technique, its speed, and cost-effectiveness. In this regard, hardware solutions can be rolled out since the additional components can increase both the complexity and the cost of the converter. On the other hand, dealing with short circuit faults require infinitely fast detection and localization, which may not be an option for the software algorithms and, consequently, the focus of this research is limited to the detection and localization of open circuit faults in MMC's power switches. The development of effective software-based fault detection and localization technique for the MMC presents considerable challenges given the redundancy in the structure and behavior of the MMC components.

## 1.3 Thesis Objectives

The objectives of the present thesis are to explore the potential of two multivariate statistical techniques, namely, the Principal Component Analysis and the Kernel Principal Component Analysis in detecting and localizing the power switches' open circuit faults in Modular Multilevel Converter. The ability of fault detection of each technique is investigated along with their ability to localize the faulty cells and the overall detection time. Besides, the thesis investigates the fault localization in terms of effectiveness, localization time and complexity of implementation under various conditions using different approaches.

## 1.4 Thesis Organization

The remainder of the thesis is structured as follows: Chapter II is dedicated to the literature review. The Modular Multilevel Converter is introduced, including its principle, design, and control. Also, efforts done to perform the fault detection and localization (FDL) in MMC are provided. Chapter III is dedicated to providing the theoretical background and modeling of the converter in hand, two commonly used control designs, and different fault detection techniques used in this thesis. Chapter VI is dedicated to the simulation results and comparison between the different techniques under the adopted control procedures. Chapter V presents the conclusions and future work.

# CHAPTER 2: LITERATURE REVIEW

## 2.1 Modular Multilevel Converter

### *2.1.1 Topology of the Modular Multilevel Converter*

Voltage source converters (VSC) are known mostly for their fast dynamic response and possibility to generate reactive power in both capacitive and inductive directions, which make them a preferable choice for medium and high voltage applications. VSCs are divided into two categories; a conventional two-level converter and multilevel converters. To achieve the voltage requirements using a two-level converter configuration and due to the physical limitations of the power electronic devices, the switches have to be connected in series. The issue that arises in this case is that the voltage change dv/dt is high when used in medium to high voltage applications, which necessitate the integration of interfacing transformers. Besides, the output voltage waveform contains more harmonics when compared to the multilevel converter case. In addition, switching losses and voltage stress on each switch is higher in the case of the two-level converters [17]. Due to the aforementioned reasons, the trend to use multilevel converters in industrial applications is rising rapidly. Along with the industrial interest, multilevel converters witnessed an increasing interest in the scientific world. One of which, the modular multilevel converter that is considered the state of the art in the multilevel converters family and which has found his way to industrial applications although its late discovery in 2001 [18].The converter structure provides valuable features that allow diversity in usage and opportunities for improvement. Although its needs in terms of switching devices and capacitors are higher than other multilevel configurations such as Flying capacitor and

cascaded H-bridge converters, it can offer higher performance as the number of levels increases [19]. Advantages of the modular multilevel converter can be depicted as follows [20],[21]:

- Modular structure
- Ability to extend the number of modules to meet power and voltage requirements
- Low voltage stress on switching devices
- Small output filters and interface transformers
- Low total harmonic distortion
- High efficiency
- Absence of dc-link capacitors
- Transformer-less or standard transformer for grid connection

On the other hand, the main disadvantage related to the MMC topology is the higher number of power semiconductors and gate units and high circulating current, which increase the probability of failures.

The increase of the industrial sector interest can be manifested in the increasing integration of the MMC in high power applications such as the Trans Bay Cable project [22] and the fact that MMC is becoming one of the compelling candidates for High Voltage DC (HVDC) transmission projects [18]. The high features offered by this converter allow its usage in other application fields such as variable speed drives[23], electric ships [24], railway power supplies [25], [26], and so on. Besides, the German Transmission System operators showed their interest to use the MMC topology for their new HVDC power transmission projects.

The topology of the MMC is as depicted in Figure 2.1. For a three-phase topology, the converter comprises three legs, each containing two arms that are connected through two identical inductors, and each arm contains $N$ submodules. The most common topology used in the submodules is the half bridge, also called the chopper-cell, which contains a capacitor and two switching devices, generally IGBTs, that are controlled by two complementary signals. The switches are unidirectional with antiparallel diodes. Accordingly, each IGBT can be either inserted or bypassed, which leads to two possible voltage output levels in the submodule; $V_{out}$ can be equal to the capacitor voltage ($+V_c$) or zero voltage depending on the switch states [27]. Hence, its simple structure renders the design and control simpler, and results in low power losses and high efficiency. Other configurations of the submodules can be applied to the MMC topology, such as the full bridge, which require twice the number of power switches to achieve the same voltage rating. However, its control and design are similar to the half bridge. Besides, it requires only the half of total dc-bus voltage to generate the same AC output voltage and has lower capacitor voltage ripples. Additional configurations of the submodules are the clamp double, the five-level cross-connected submodules, the three-level flying capacitor and the three-level neutral-point clamped. More details of the different configurations and their specifications can be found in [21],[27],[28]. The purpose of deploying the arm inductors is to protect the converter during short circuit faults. Also, they damp the rising currents in case of asymmetric operations.

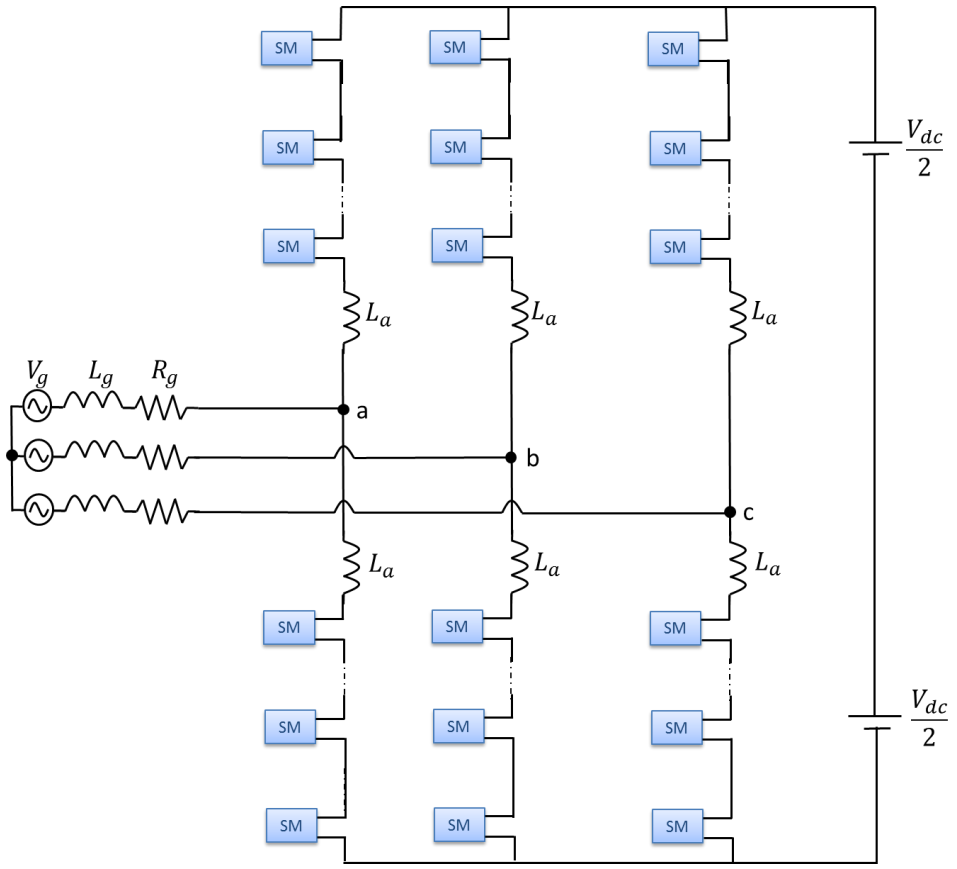


Figure 2.1: Three phase Modular Multilevel Converter.

In the current thesis, the conventional half bridge submodule is used in the study and simulations. The output voltage of the converter is synthesized through the number of inserted and bypassed of the series connected submodules in the upper and lower arms.

The submodules have three operating modes as shown in Figure 2.2:

- Blocking or energizing mode: where both switches are turned off, and it is used to charge the capacitors depending on the direction of the current. This mode cannot exist under normal operating conditions since, as mentioned before, the two switches are inserted complimentarily.
- Put-in or capacitor ON mode: where the upper switch is turned ON, and the lower switch is turned OFF. In this case, the IGBT conducts when the current flows out of the submodule and the capacitor discharges and when the current flows in the reverse direction the antiparallel diode conducts and the capacitor charges. The output of the cell is equal to $V_c$.
- Put-out or capacitor OFF mode: where the upper switch is turned OFF, and the lower switch is turned ON. In this case, The IGBT conducts when the current flows inside the cell, and the antiparallel diode conducts when the current flows in the reverse direction, and within both cases, the capacitor maintains its previous state. The output of the cell is equal to zero.

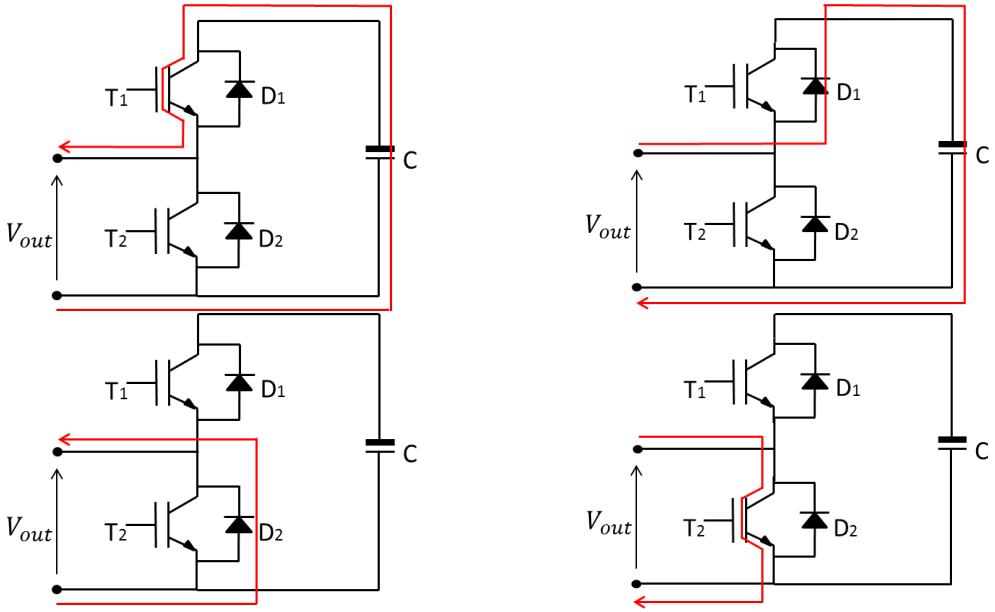


Figure 2.2: Put-in, Put-out operation modes of the submodules

### *2.1.2 Design of the Modular Multilevel Converter*

The capacitors and the inductors should satisfy specific criteria to achieve the optimal operational performance of the converter [29]. The capacitance of the submodule capacitor is selected such that an acceptable capacitor voltage ripples are obtained. As previously mentioned, the capacitors are charged and discharged based on the switching patterns and direction of the arm currents. The circulating currents that circulate the arms yield voltage ripples in the capacitor voltage, which cannot be suppressed however they can be reduced by proper choice of the capacitance.

The relationship between the capacitance and the voltage ripples is depicted in Equation (2.1) as follows:

$$C = \frac{S}{3NmE_{avg}\Delta e_c \omega_c}\left(1 - \left(\frac{mcos\phi}{2}\right)^2\right)^{3/2} \quad (2.1)$$

Where *S* is the apparent power, *N* is the number of submodules per arm, *m* is the modulation index, $E_{avg}$ is the average capacitor voltage, $cos\phi$ is the power factor and $\omega_c$ is the control frequency.

The arm inductor is crucial for filtering the output current ripples and isolate the two arms of the leg. The inductance of the arm inductors should satisfy the relationship depicted in Equation (2.2).

$$L_a C > \frac{5N}{48\omega^2} \quad (2.2)$$

### *2.1.3 Control of the Modular Multilevel Converter*

Several techniques were proposed in the literature to control the MMC [29]–[42] that can be broadly classified into Pulse Width Modulated (PWM) techniques and sorting techniques. The control strategy is a crucial task since, if not appropriately set, the imbalance between the arms can lead to severe results. Therefore, the goal of the control in the MMC is to assure the balancing of the capacitor voltages, reduce the circulating current along with assuring a proper output voltage and current waveforms.

PWM controllers are widely accepted in the power converters control. The output signal is generated through controlling the duty cycle of the power switches. A multitude of schemes exists in the literature of the PWM techniques [43]–[48], which are designed to reduce the harmonic distortion, current ripples and the power losses along with

maintaining an acceptable capacitor voltage levels. They can be categorized into high switching frequency, fundamental switching frequency, and low switching frequency modulation schemes. The most used PWM schemes are the multicarrier modulation schemes, which are divided into two categories, namely, the phase-shifted carrier PWM and the level-shifted carrier PWM. A large variety of techniques are using either voltage oriented control, which is generally accepted in HVDC applications [49], or current oriented control such as the case of STATCOM to meet the reactive power requirements [50]. Other techniques are also used to control the MMC including the submodule capacitor voltage control, circulating current control and the model predictive control that have been extensively elaborated in the literature. Two control techniques are used in this thesis; a PWM-based voltage-balancing technique and a predictive control based technique. The usage of two different control schemes along with different converter size gives an insight into the robustness of each technique and the complexity of the fault detection in each case.

## 2.2 Fault Detection and Localization in MMC

The MMC specific structure allows the use of commercial switches and capacitors [19], which reduce the cost of the converter. However, the need for having a higher number of levels to satisfy the power and voltage requirements increases the number of cells, and consequently, the complexity of the converter and the control design, and the risk of malfunctions and failures.

Power switches, as one of the most vulnerable components in MMC, are subject to different kind of deficiencies and faults, which can severely affect the system and lead to unstable working conditions and shutdowns [15].

Failures in power switches can occur in three forms: miscommunication between gate drives and switches, short circuit, and open circuit faults [16]. The loss of connection between gate drives and power switches can be seen as open circuit faults. To isolate them, smart gate drives capable of detecting the connection status have been widely used. On the other hand, short circuit faults are destructive and have to be detected and dealt with in a short time [51] since it leads to rapid discharge of the capacitor associated with the faulty switch, and thus the two complementary devices cannot be protected against the shoot-through faults [52]. Similar to the gate drives misfiring, the most used techniques to address the short circuit faults is through hardware implementation. Nevertheless, some efforts were made in the detection of short circuit faults using software techniques [53],[54]. Open circuit faults occur when the power switch fails to change its state to be ON and acts as an open circuit. As a direct consequence, the corresponding capacitor voltage keeps increasing, which creates an unbalance between the upper and lower arm capacitor voltages, higher circulating current, and distorted output voltage. If the detection technique is fast enough, the detection and isolation of such faults can be assured.

The detection of faults and their localization can be addressed by either hardware [55]-[56] or software implementations [42], [57]–[72]. In the hardware implementation, additional hardware components, such as redundant switches and sensors, are required to identify and mitigate the malfunctioning devices. Whereas software-based techniques can be broadly divided into two groups, namely, the model-based techniques [54], [56], [61]–[64], [66], [67], [69], [73], [74] in which the mathematical model of the system is used, and data-driven techniques [53] that uses the general behavior of the system.

An extensive focus was given to the sliding mode observers (SMO) [64], [65], [69], [74]. In [66], estimated variables using Kalman filter are compared to the measured states to perform the fault detection. In [62] an extended state observer to track the arm current is used as fault detection indicator. In [72], a change in the measurement from the capacitor voltage to the cell output voltage along with the usage of an XOR unit is deployed to detect single and multiple open circuit and short circuit faults. In [53], a neural network technique is used for fault detection in a seven-level MMC. A voltage based detection approach to detect and localize single open circuit fault in MMC was introduced in [75], where a threshold defines the absolute error margin between the measured and the predicted values of the sum and difference between the upper and lower arm voltages, beyond which the system can be considered faulty if the fault persists for more than $0.5ms$. Based on the signs of the normalized sum and difference, the faulty switch position can be narrowed to one quarter of the possible locations. The set of possible fault sites is then constructed and a counter that adds weight to the combination that results in estimation error and subtract it from the combination that results in low error is then used to identify the exact location of the faulty switch that eventually ends up by having the largest weight. It has been reported that this technique is able to isolate, on average, the faulty cell within 4.58 periods when the number of submodules is 10 and in 7.96 periods when 100 submodules are considered. This technique, however, can only detect one fault at a time and is only applicable to model predictive controls. Authors in [76] Suggest that correlating the output voltage level with the modulation index gives an insight of the faulty states of the system. Besides, the usage of additional submodules, such that the redundant cells are included in the control scheme and the working cells are grouped in rotating sequences, should eventually isolate the cell

with the faulty switch by finding the combination that correspond to the normal working conditions of the MMC. An Adaptive Linear Neuron (ADALINE) algorithm is introduced in [77]. It correlates the switching states by a linear combination with some weighting factor, which is updated with the Widrow-Hoff delta rule adaptation algorithm. A faulty state is detected if the per-unit voltage gets below 85%. The rate of change of the difference between the outputs estimated by the ADALINE and the Recursive Least Squares (RLS) algorithm is then compared to a predefined threshold and allows the fault localization. The algorithm is capable of detecting multiple faults. Another multiple fault detection method is used in [78], where a modification in the location of the sensors monitoring the capacitor voltages is proposed in order to measure the submodule terminals. The fault detection and localization is based on a combination between the sampling instance, arm current direction and the terminal voltage. Besides, the monitoring is local for each cell, and is done simultaneously in real time which decreases significantly the detection time. In [79], a multi-step prediction method is used to elaborate an improved circulating current prediction algorithm that is useful in eliminating the uncertainties and disturbances that can occur to the measurements. This current estimate is then compared to the measured value and a threshold is used to identify the normal operation conditions. The localization is performed using a threshold on the capacitor voltages.

# CHAPTER 3: MMC CONTROL AND PROPOSED FAULT DETECTION AND LOCALIZATION METHODOLOGIES

## 3.1 Introduction

A large variety of control techniques has been proposed in the literature to control the MMC. As the primary concern of this thesis is to provide a fault detection and localization technique to monitor the open circuit faults in the power switches, the role of the control in the process of the fault detection and localization should be investigated since the stiffness of a control algorithm may interfere with the process of fault detection and localization. To this end, two popular control techniques that belong to two different control families have been adopted; the Model Predictive Control (MPC), which is a sorting technique that is set to optimize a cost function by inserting and bypassing the submodules of the MMC, and consequently gives the optimum combination that allows best tracking and balancing of the system. The second technique is based on the PWM-based voltage-balancing control, which, in contrast to the current reference in the sorting technique, has a voltage reference and uses a phase shifted carrier to generate the switching signals. Detailed descriptions of the adopted approaches are given in the following sections.

## 3.2 Mathematical Model of the MMC

Prior to the control design and formulation of fault detection procedures, the elaboration of the mathematical model of the system is crucial and to do so a single phase topology is used.

Figure 3.1 shows a four half bridge cells, single phase MMC, where the two switches of each cell alter their state complementarily, the arms are equipped with inductors, and the load is an RL load.

The relationship between different parameters of the converter can be elaborated using Kirchhoff's law as stated by Equations (3.1)-(3.5), where

- $E_1$, $E_2$, $E_3$, $E_4$ represent the capacitor voltages of the converter
- $U_1, U_2, U_3, U_4, \overline{U}_1, \overline{U}_2, \overline{U}_3, \overline{U}_4$ represent the switching states of the upper and lower switches of the cells, respectively.
- $i_{up}, i_{down}$ represent the upper and lower arms currents, respectively.
- $V_{dc}$ is the dc source.
- $i_L, i_{diff}$ are the load and circulating currents, respectively.
- $L$, $R$ are the inductance and the resistance of the arm inductor
- $L_L$, $R_L$ are the inductance and resistance of the load
- $C$ is the cells' capacitor

$$V_{dc} = U_1E_1 + U_2E_2 + L\frac{di_{up}}{dt} + Ri_{up} - L\frac{di_{down}}{dt} - Ri_{down} + U_3E_3 + U_4E_4 \tag{3.1}$$

$$\frac{1}{2}V_{dc} = U_1E_1 + U_2E_2 + L\frac{di_{up}}{dt} + Ri_{up} + L_L\frac{di_L}{dt} + R_Li_L \tag{3.2}$$

$$\frac{1}{2}V_{dc} = U_3E_3 + U_4E_4 - L\frac{di_{down}}{dt} - Ri_{down} - L_L\frac{di_L}{dt} - R_Li_L \tag{3.3}$$

$$i_{up} = \frac{i_L}{2} + i_{diff}, \qquad i_{down} = \frac{i_L}{2} - i_{diff} \tag{3.4}$$

$$\frac{dE_1}{dt} = \frac{U_1}{C}\left(\frac{i_L}{2} + i_{diff}\right), \qquad \frac{dE_2}{dt} = \frac{U_2}{C}\left(\frac{i_L}{2} + i_{diff}\right)$$

$$\frac{dE_3}{dt} = \frac{U_3}{C}\left(-\frac{i_L}{2} + i_{diff}\right), \qquad \frac{dE_4}{dt} = \frac{U_4}{C}\left(-\frac{i_L}{2} + i_{diff}\right) \tag{3.5}$$

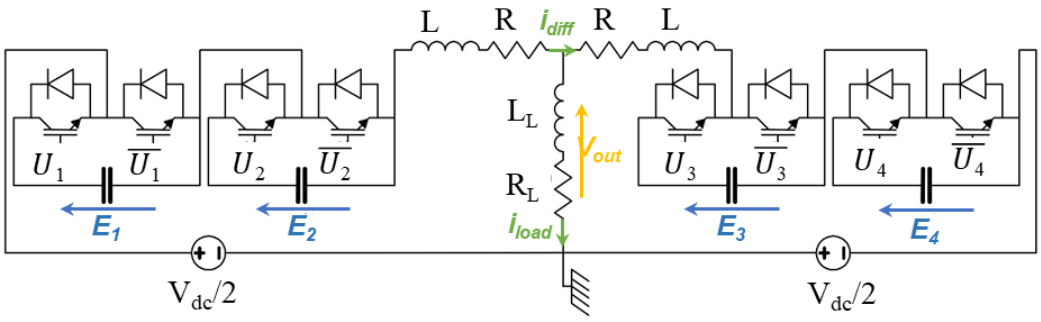


Figure 3.1: Topology of a four cells single phase MMC

The state space equation corresponding to the four cells MMC can be described by the following state-space equation (3.6)

$$\begin{bmatrix} \frac{di_{diff}}{dt} \\ \frac{dE1}{dt} \\ \frac{dE2}{dt} \\ \frac{dE3}{dt} \\ \frac{dE4}{dt} \\ \frac{di_{load}}{dt} \end{bmatrix} = \begin{bmatrix} -\frac{R}{L} & -\frac{U_1}{2L} & -\frac{U_2}{2L} & -\frac{U_3}{2L} & -\frac{U_4}{2L} & 0 \\ \frac{U_1}{C} & 0 & 0 & 0 & 0 & \frac{U_1}{2C} \\ \frac{U_2}{C} & 0 & 0 & 0 & 0 & \frac{U_2}{2C} \\ \frac{U_3}{C} & 0 & 0 & 0 & 0 & -\frac{U_3}{2C} \\ \frac{U_4}{C} & 0 & 0 & 0 & 0 & -\frac{U_4}{2C} \\ 0 & -\frac{U_1}{L+2L_L} & -\frac{U_2}{L+2L_L} & \frac{U_3}{L+2L_L} & \frac{U_4}{L+2L_L} & -\frac{R+2R_L}{L+2L_L} \end{bmatrix} \begin{bmatrix} i_{diff} \\ E_1 \\ E_2 \\ E_3 \\ E_4 \\ i_{load} \end{bmatrix} + \begin{bmatrix} \frac{V_{dc}}{2L} \\ 0 \\ 0 \\ 0 \\ 0 \\ 0 \end{bmatrix} \quad (3.6)$$

## 3.3 Model Predictive Control

The ultimate goal of MMC control is to track an output reference signal. However, to do so, other challenges such as maintaining the capacitor voltages at a predefined level $\left(\frac{V_{dc}}{N}\right)$ and minimizing the circulating current should also be addressed. The circulating current is the current that flows between the converter and the dc source. Consequently, it does not reach the load. This current is caused by the unbalance between the two arm currents and, it affects the ripples in the capacitor voltages alongside the ratings of the used components.

Therefore, the cost function to be optimized by the predictive control should take these constraints into account to obtain the best switching pattern. To alleviate the effect the large variance differences between different parameters, which would bias the output of the cost function, the measured data should be normalized.

Besides, additional weights are added to some parameters in order to achieve better tracking and stability [38]. Hence, the cost function to be optimized is as described in Equation (3.7);

$$\min \sqrt{\left(\frac{i_{diffref} - i_{diff}}{\lambda \Delta i_{diff}}\right)^2 + \left(\frac{E_{kref} - E_k}{\Delta E_k}\right)^2 + \left(\frac{i_{Lref} - i_L}{\beta \Delta i_L}\right)^2}, \qquad (3.7)$$

$$k = 1 \ldots 4$$

Where $\Delta parameter = |\max(prameter(k+1)) - \min(parameter(k+1))|$,

$parameter = i_{diff}, E_k, i_L,\ i_{diffref} = 0,\ E_k = \frac{V_{dc}}{N},\ \lambda, \beta: weighting\ factors$

The algorithm of the MPC control is illustrated in Figure 3.2 and is described as follows;

- Measure the state variables described by the state space equation (3.6), which includes the capacitor voltages $E_1 \ldots E_k$, the circulating current $i_{diff}$ and the load current $i_L$.
- Calculate the future states using all possible switching patterns and corresponding cost functions such that the update of the possible state is calculated in Equation (3.8)

$$X_i(k+1) = X(k) + \dot{X}_i(k) T_s \qquad (3.8)$$

  where $i$=1…number of possible switching pattern (sequences), $T_s$ is the sampling period, and $X(k)$ represents the vector of the measured variables.
- Perform the optimization process to choose the switching pattern that corresponds to the minimum error between the references and the predictions.

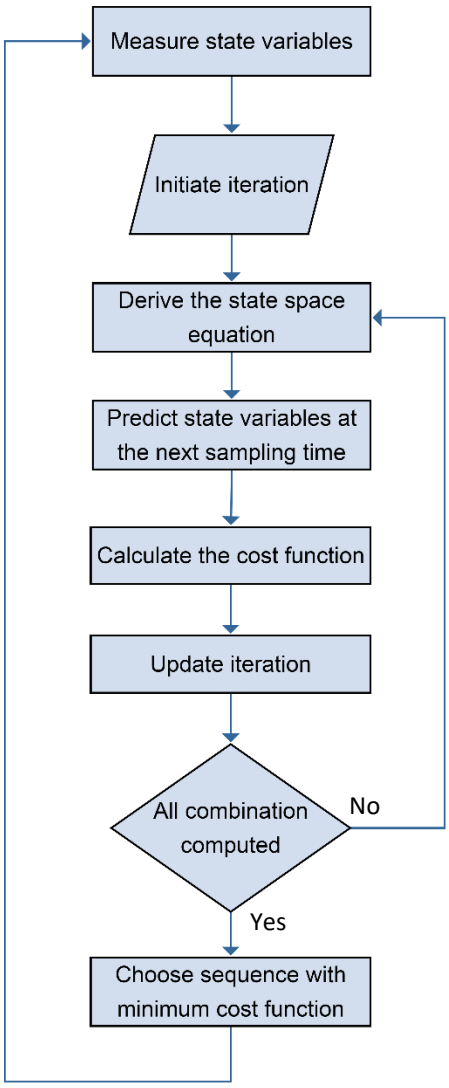


Figure 3.2: Flowchart of the Predictive control algorithm

## 3.4 PWM-Based Voltage-Balancing Control

Among the control goals are keeping the stored energy inside the cell capacitors at a certain level, or equivalently, the average capacitor voltage should be kept at the desired reference is one of the control goals. Besides, the voltage level for each cell capacitor should be kept around a reference value. To control the MMC using the PWM technique, a voltage-balancing approach is considered [33]. The selection of the switching sequence is based on the phase-shifted PWM, and the control design is based on two loops in which an averaging control and a balancing control are considered. Open loop control is used to track the AC voltage reference.

### *3.4.1 Averaging Control*

In the averaging control, two PI controllers are used to control the average capacitor voltages and the circulating current as shown in Figure 3.3. The average capacitor voltage is given by Equation (3.9)

$$E_{avg} = \frac{1}{N}\sum_{k=1}^{N} E_k \tag{3.9}$$

The circulating current reference signal is obtained using the first PI command, and it is given by Equation (3.10)

$$i_{diffref} = K_1\left(E_{ref} - E_{avg}\right) + K_2 \int \left(E_{ref} - E_{avg}\right)dt \tag{3.10}$$

The voltage command reference is given using the second PI output and it is given by Equation (3.11)

$$V_{avgref} = K_3\left(i_{diff} - i_{diffref}\right) + K_4 \int \left(i_{diff} - i_{diffref}\right)dt \qquad (3.11)$$

The controller forces the circulating current to follow its reference, and ultimately the average control approaches its reference signal when the steady state is reached.

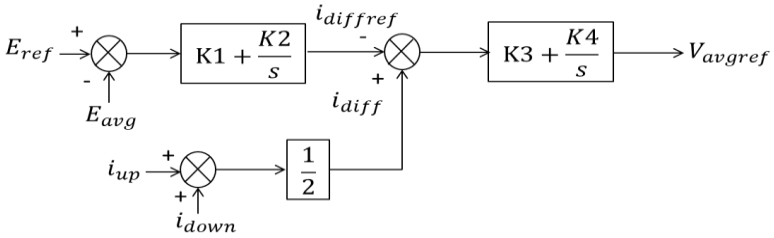


Figure 3.3: Block diagram of the averaging control

### *3.4.2 Balancing Control*

The role of the balancing control is to bring the individual cells' capacitor voltages to the desired level. The sign of the difference between the capacitor voltage reference and the actual capacitor voltage of each cell gives an insight about whether or not a positive power should be taken from the *dc* source and injected in the cells. However, when the arm current changes its direction, the corresponding error should also change its sign to keep a

resulting positive power that will be injected into the cells. Therefore, the controller should consider the current direction to perform the balancing control.

Figure 3.4 illustrates the balancing control block diagram. The output of the balancing control is represented as Equation (3.12)

$$V_{balref} = \begin{cases} K_5(E_{ref} - E_k) & i_{up}, i_{down} > 0 \\ -K_5(E_{ref} - E_k) & i_{up}, i_{down} < 0 \end{cases} \quad (3.12)$$

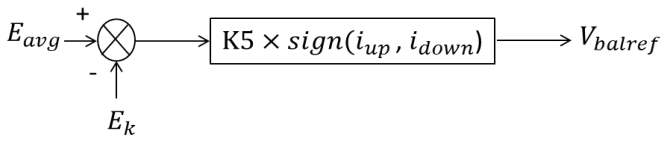


Figure 3.4: Block diagram of the balancing control

For each cell, the voltage command resultant from the two control loops is added and compared with the output voltage reference signal (the upper arm is compared with the reference signal over the number of cells per arm $\left(\frac{V_{outref}}{N}\right)$ and the lower arm is compared with the opposite of the reference signal over the number of cells per arm $\left(-\frac{V_{outref}}{N}\right)$) . Besides, a feedforward of the dc power supply $\left(\frac{E}{2N}\right)$ is also added in order to compensate the dc disturbances as shown in Figure 3.5.

The output of the upper and lower arm commands are represented as Equations (3.13) and (3.14):

$$V_{up} = V_{avgref} + V_{balref} - \frac{V_{outref}}{N} + \frac{E}{2N} \text{ (upper arm cells)} \quad (3.13)$$

$$V_{down} = V_{avgref} + V_{balref} + \frac{V_{outref}}{N} + \frac{E}{2N} \text{ (lower arm cells)} \quad (3.14)$$

Finally, to get the appropriate switching pattern, the resultant voltage commands are then normalized by each capacitor voltage $E_k$ and compared to $N$ triangular phase-shifted carriers with the same frequency and having a unity maximum and a minimum of zero.

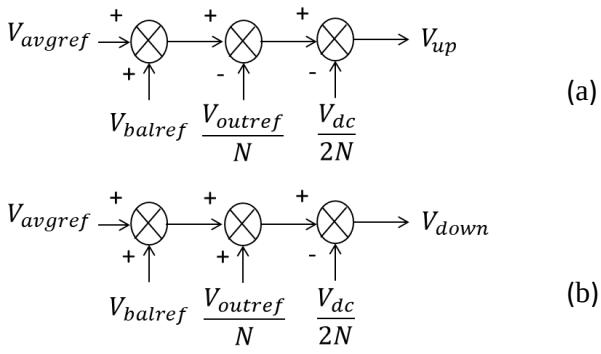


Figure 3.5: Output commands for (a) upper arm and (b) lower arm

## 3.5 Fault Formulation in MMC

To understand the normal behavior and faulty states of the MMC, an in-depth look at the effect of open circuit faults on the system dynamics is needed. The normal operation conditions, as depicted in Table 3.1 [80], states that the capacitor is charged when the upper switch $T_1$ of the submodule is inserted, and the arm current is flowing outward the cell (from the negative side to the positive side of the cell capacitor). Similarly, the capacitor is discharged when the upper switch $T_1$ of the submodule is inserted, and the arm current flows inward. In the case, the lower switch of the submodule is inserted the cell is bypassed, and the capacitor keeps its previous status regardless of the arm's current direction. When a single open circuit fault surges, two fault scenarios are considered. Namely, the faulty power switch is located either in the upper side of the submodule or the lower side. In the case of upper switch $T_1$ open circuit fault, the cell capacitor keeps charging without any possibility of discharge since charging procedure occurs when the current is flowing outwards through the freewheel diode, that is supposed intact and still working correctly, while the open circuit fault prevents the capacitor from discharging. Besides, the submodule output voltage is equal to the capacitor voltage only when the switch $T_1$ is ON, and the current is flowing inwards meaning that the capacitor voltage keeps increasing and subsequently each time this condition occurs the dynamic of the whole system is affected. In contrast, in case of lower switch $T_2$ open circuit fault, the cell capacitor keeps charging regardless of the gating signal when the current is positive (the current is directed towards the submodule), and it works as expected when the current is negative. Similarly, the resultant behavior, in this case, forces the capacitor voltage to keep increasing since the

charging period is higher than the discharging period. Besides, the submodule output is equal to the capacitor voltage in three out of four cases which results in disrupting the normal operation of the converter.

To further study the effect of the fault in the dynamics of the system, the state space equation derived earlier is rewritten and the analysis of fault impact is performed on a four cell MMC.

In the normal working conditions, the state space equation can be formulated using Kirchhoff's laws. For a four-cell system in normal conditions, the state space equation is as depicted in Equation (3.15).

$$\begin{bmatrix} \frac{di_{diff}}{dt} \\ \frac{dE1}{dt} \\ \frac{dE2}{dt} \\ \frac{dE3}{dt} \\ \frac{dE4}{dt} \\ \frac{di_{load}}{dt} \end{bmatrix} = \begin{bmatrix} -\frac{R}{L} & -\frac{U_1}{2L} & -\frac{U_2}{2L} & -\frac{U_3}{2L} & -\frac{U_4}{2L} & 0 \\ \frac{U_1}{C} & 0 & 0 & 0 & 0 & \frac{U_1}{2C} \\ \frac{U_2}{C} & 0 & 0 & 0 & 0 & \frac{U_2}{2C} \\ \frac{U_3}{C} & 0 & 0 & 0 & 0 & -\frac{U_3}{2C} \\ \frac{U_4}{C} & 0 & 0 & 0 & 0 & -\frac{U_4}{2C} \\ 0 & -\frac{U_1}{L+2L_L} & -\frac{U_2}{L+2L_L} & \frac{U_3}{L+2L_L} & \frac{U_4}{L+2L_L} & -\frac{R+2R_L}{L+2L_L} \end{bmatrix} \begin{bmatrix} i_{diff} \\ E_1 \\ E_2 \\ E_3 \\ E_4 \\ i_{load} \end{bmatrix} + \begin{bmatrix} \frac{V_{dc}}{2L} \\ 0 \\ 0 \\ 0 \\ 0 \\ 0 \end{bmatrix} \quad (3.15)$$

The equations that lead to the aforementioned state space are derived supposing that in the typical case the output voltage of the cell is always equal to $U_k E_k$ where $U_k$ is the gate signal and it is equal to 1 when the upper switch of the cell is inserted and the lower switch is bypassed and equal to 0 in the inverse situation. $E_k$ is the voltage measured across the corresponding capacitor $C_k$. The normal working conditions of a power switch is depicted in Figure 2.2 where the cell's output voltage is a function of the switch state and the crossing current direction. As shown in the Table 3.1 the cell's output voltage is equal to the product of the switch input signal $U_k$ by the corresponding capacitor voltage.

In case of open circuit fault occurrence, the total system is affected, and the output voltage of the affected cells is no longer equal to the value $U_k E_k$.

Table 3.1: Cell voltage output in normal and faulty cases

| Status | Current Direction $i_{arm}$ | Gate signal $U_k$ | Output voltage | Capacitor status |
|---|---|---|---|---|
| Normal case | + | 1 | $E_k$ | Charge |
| | | 0 | 0 | Bypass |
| | - | 1 | $E_k$ | Discharge |
| | | 0 | 0 | Bypass |
| Open circuit in $T_1$ | + | 1 | $E_k$ | Charge |
| | | 0 | 0 | Bypass |
| | - | 1 | 0 | Bypass |
| | | 0 | 0 | Bypass |
| Open circuit in $T_2$ | + | 1 | $E_k$ | Charge |
| | | 0 | $E_k$ | Charge |
| | - | 1 | $E_k$ | Discharge |
| | | 0 | 0 | Bypass |

It can be seen, from Table 3.1, that the output voltage of the affected cell has two different Equations (3.16) and (3.17) depending on the fault location. Therefore, we can formulate the output voltage of the capacitor voltages based on additional terms that take fault effects into consideration.

The output voltage of the affected cell can be elaborated as;

- Case 1: The open circuit fault affects the upper switch $T_1$ of a given cell $k$

$$\frac{sign(i_x)+1}{2}U_k \text{ given that } i_x \neq 0 \tag{3.16}$$

- Case 2: The open circuit fault affects the upper switch $T_2$ of a given cell $k$

$$\frac{sign(i_x)+1}{2}+U_k-\frac{sign(i_x)+1}{2}U_k \text{ given that } i_x \neq 0 \tag{3.17}$$

where $i_x$ represent the upper arm current or the lower arm current of the corresponding faulty cell.

A faulty condition state space equation is derived using the Kirchhoff's laws by replacing the faulty cell's voltage by the corresponding expression stated above. In the case of a four-cell converter, the number of possible single fault conditions is eight. Thus eight additional equations are added to the original state space equation.

The formulation of a faulty switch $T_1$ in the upper cell $E_1$ is derived as follows:

According to Kirchhoff's laws, we can elaborate the Equations (3.18)-(3.22).

$$V_{dc}=\frac{sign(i_{up})+1}{2}U_1E_1+U_2E_2+L\frac{\partial i_{up}}{\partial t}+Ri_{up}-L\frac{\partial i_{down}}{\partial t} - Ri_{down}+U_3E_3+U_4E_4 \tag{3.18}$$

$$\frac{V_{dc}}{2}=\frac{sign(i_{up})+1}{2}U_1E_1+U_2E_2+L\frac{\partial i_{up}}{\partial t}+RI_{up}+L_L\frac{\partial i_L}{\partial t}+R_Li_L \tag{3.19}$$

$$\frac{V_{dc}}{2}=U_3E_3+U_4E_4-L\frac{\partial i_{down}}{\partial t}-Ri_{down}-L_L\frac{\partial i_L}{\partial t}-R_Li_L \tag{3.20}$$

$$i_{up}=\frac{i_L}{2}+i_{diff} \qquad i_{down}=\frac{i_L}{2}-i_{diff} \tag{3.21}$$

$$\frac{\partial E_1}{\partial t} = \frac{\left(sign\left(i_{up}\right)+1\right)}{2C} U_1 \left(\frac{i_L}{2} + i_{diff}\right); \frac{\partial E_2}{\partial t} = \frac{U_2}{C}\left(\frac{i_L}{2} + i_{diff}\right);$$
$$\frac{\partial E_3}{\partial t} = \frac{U_3}{C}\left(\frac{-i_L}{2} + i_{diff}\right); \frac{\partial E_4}{\partial t} = \frac{U_4}{C}\left(\frac{-i_L}{2} + i_{diff}\right) \quad (3.22)$$

Using the Equations (3.18)-(3.22) the relation between the state variables can be constructed in the same manner as the normal case as illustrated in Equations (3.23)-(3.28).

(1)&(4) ⇒

$$V_{dc} = \frac{\left(sign(i_{up})+1\right)}{2} U_1 E_1 + U_2 E_2 + 2L\frac{\partial i_{diff}}{\partial t} + 2R i_{diff} + U_3 E_3 + U_4 E_4 \quad (3.23)$$

$$\frac{\partial i_{diff}}{\partial t} = \frac{V_{dc}}{2L} - \frac{R}{L} i_{diff} - \frac{U_1}{4L}\left(sign(i_{up})+1\right)E_1 - \frac{U_2}{2L}E_2 - \frac{U_3}{2L}E_3 - \frac{U_4}{2L}E_4 \quad (3.24)$$

(2) − (3) ⇒

$$0 = \frac{\left(sign(i_{up})+1\right)}{2} U_1 E_1 + U_2 E_2 + 2L\frac{\partial i_{diff}}{\partial t} + 2R i_{diff} - U_3 E_3 - U_4 E_4 + 2L_L\frac{\partial i_L}{\partial t} + 2R_L i_L \quad (3.25)$$

(2)&(4) ⇒

$$\frac{V_{dc}}{2} = \frac{\left(sign(i_{up})+1\right)}{2} U_1 E_1 + U_2 E_2 + \frac{L}{2}\frac{\partial i_L}{\partial t} + L\frac{\partial i_{diff}}{\partial t} + \frac{R}{2} i_L + R i_{diff} + L_L\frac{\partial i_L}{\partial t} + R_L i_L \quad (3.26)$$

(3)&(4) ⇒

$$\frac{V_{dc}}{2} = U_3 E_3 + U_4 E_4 - \frac{L}{2}\frac{\partial i_L}{\partial t} + L\frac{\partial i_{diff}}{\partial t} - \frac{R}{2} i_L + R i_{diff} - L_L\frac{\partial i_L}{\partial t} - R_L i_L \quad (3.27)$$

$(8) - (9) \Rightarrow$

$$0 = \frac{\left(sign(i_{up}) + 1\right)}{2} U_1 E_1 + U_2 E_2 + (L + 2L_L)\frac{\partial i_L}{\partial t} + (R + 2R) i_L - U_3 E_3 - U_4 E_4 \tag{3.28}$$

Proceeding in the same manner yields the below state space equation that includes all faults

$$\begin{bmatrix} \frac{di_{diff}}{dt} \\ \frac{dE1}{dt} \\ \frac{dE2}{dt} \\ \frac{dE3}{dt} \\ \frac{dE4}{dt} \\ \frac{di_{load}}{dt} \end{bmatrix} = \begin{bmatrix} -\frac{R}{L} & -\frac{U_1}{2L} & -\frac{U_2}{2L} & -\frac{U_3}{2L} & -\frac{U_4}{2L} & 0 \\ \frac{U_1}{C} & 0 & 0 & 0 & 0 & \frac{U_1}{2C} \\ \frac{U_2}{C} & 0 & 0 & 0 & 0 & \frac{U_2}{2C} \\ \frac{U_3}{C} & 0 & 0 & 0 & 0 & -\frac{U_3}{2C} \\ \frac{U_4}{C} & 0 & 0 & 0 & 0 & -\frac{U_4}{2C} \\ 0 & -\frac{U_1}{L+2L_L} & -\frac{U_2}{L+2L_L} & \frac{U_3}{L+2L_L} & \frac{U_4}{L+2L_L} & -\frac{R+2R_L}{L+2L_L} \end{bmatrix} \begin{bmatrix} i_{diff} \\ E_1 \\ E_2 \\ E_3 \\ E_4 \\ i_{load} \end{bmatrix} +$$

$$\begin{bmatrix} \frac{V_{dc}}{2L} \\ 0 \\ 0 \\ 0 \\ 0 \\ 0 \end{bmatrix} + \begin{bmatrix} -(\text{sign}(i_{up})-1)\frac{E_1}{4L} \\ (|i_{up}|-i_{up})\frac{1}{2C} \\ 0 \\ 0 \\ 0 \\ -(\text{sign}(i_{up})-1)\frac{E_1}{2L+4L_L} \end{bmatrix} U_1 f_1 + \begin{bmatrix} -(\text{sign}(i_{up})-1)\frac{E_2}{4L} \\ 0 \\ (|i_{up}|-i_{up})\frac{1}{2C} \\ 0 \\ 0 \\ -(\text{sign}(i_{up})-1)\frac{E_2}{2L+4L_L} \end{bmatrix} U_2 f_2$$

$$+ \begin{bmatrix} -(\text{sign}(i_{down})-1)\frac{E_3}{4L} \\ 0 \\ 0 \\ -(|i_{down}|-i_{down})\frac{1}{2C} \\ 0 \\ (\text{sign}(i_{down})-1)\frac{E_3}{2L+4L_L} \end{bmatrix} U_3 f_3 + \begin{bmatrix} -(\text{sign}(i_{down})-1)\frac{E_4}{4L} \\ 0 \\ 0 \\ 0 \\ -(|i_{down}|-i_{down})\frac{1}{2C} \\ (\text{sign}(i_{down})-1)\frac{E_4}{2L+4L_L} \end{bmatrix} U_4 f_4 \qquad (3.29)$$

$$+ \begin{bmatrix} -(\text{sign}(i_{up})+1)\frac{E_1}{4L} \\ (|i_{up}|+i_{up})\frac{1}{2C} \\ 0 \\ 0 \\ 0 \\ -(\text{sign}(i_{up})+1)\frac{E_1}{2L+4L_L} \end{bmatrix} (1-U_1) f_5 + \begin{bmatrix} -(\text{sign}(i_{up})+1)\frac{E_2}{4L} \\ 0 \\ (|i_{up}|+i_{up})\frac{1}{2C} \\ 0 \\ 0 \\ -(\text{sign}(i_{up})+1)\frac{E_2}{2L+4L_L} \end{bmatrix} (1-U_2) f_6$$

$$+ \begin{bmatrix} -(\text{sign}(i_{down})+1)\frac{E_3}{4L} \\ 0 \\ 0 \\ -(|i_{down}|+i_{down})\frac{1}{2C} \\ 0 \\ (\text{sign}(i_{down})+1)\frac{E_3}{2L+4L_L} \end{bmatrix} (1-U_3) f_7 + \begin{bmatrix} -(\text{sign}(i_{down})+1)\frac{E_4}{4L} \\ 0 \\ 0 \\ 0 \\ -(|i_{down}|+i_{down})\frac{1}{2C} \\ (\text{sign}(i_{down})+1)\frac{E_4}{2L+4L_L} \end{bmatrix} (1-U_4) f_8$$

where $f_1, f_2, f_3, f_4$ represent the faults occurring in the upper switch $T_1$ of each cell, and $f_5, f_6, f_7, f_8$ represent the fault effect when occurring in the lower switch $T_2$ in each cell. Meaning that if the fault is occurring in the upper switch of cell 1 located in the upper arm, $f_1$ will take the value 1 and the corresponding equation will be added to the system. As it can be seen from the Equation (3.29), the state space equation is written in the form of Equation (3.30)

$$\dot{x} = A(U)x + D + \sum_{i=1}^{8} lf \tag{3.30}$$

The state space equation (3.29) derived for open circuit faults shows that the fault affects the corresponding capacitor voltage along with the load current and the circulating current. However, the fault propagation to the remaining capacitor voltage is done via the dynamics of the system. Thus, indications about the converter pattern under single open circuit faults can be derived using either the full state variables or using only the capacitor voltages.

## 3.6 Proposed Fault Detection Techniques

### *3.6.1 Principal Component Analysis*

Principal component analysis (PCA) is a statistical technique that was invented in 1889, but its research and applications are still used up to date in a variety of applications, including fault detection [81]–[83].

PCA is a dimensionality reduction procedure in which datasets with large dimension are reduced to lower dimension space by keeping the essential features, named as principal components that account for the largest variability of the data in the original higher dimension [84], [85]. In other words, the PCA approach eliminates the redundancy existing in the original data, and it creates a new artificial set of data, which does not have any physical meaning by itself, but it regroups the correlated variables and thus making the relations between variables more clear. In fact, it can be seen as the linear projection of the state variables into new lower dimensions to be better presented and more analyzable.

The PCA procedure seeks the orthogonal axes that maximize the scatter of the data, which will allow the separation of the data when projected into this new dimension [86]. The main reason to use this data-driven technique in this thesis is that it does not require prior knowledge of the mathematical model of the system. Besides, the open circuit fault is abrupt, meaning that the system behavior after fault occurrence shows total divergence from the normal working conditions, and considering the capacity of the PCA to detect abnormalities in patterns, it can be effective for fault detection in MMC. In addition, once the training is performed, the online monitoring does not require extensive calculations, which makes it very fast in detecting faults.

Consider the dataset $X = [x_1\ x_2\ ...\ x_N]^T$, where $x_i = \left[x_{i1}\ x_{i2}\ ...\ x_{ip}\right]^T$ a $p$-dimensional vector. PCA will perform a projection into a lower dimension vector such that the projection would be as illustrated in Equation (3.31)

$$y_i = Ax_i \tag{3.31}$$

where $A = \left[u_1^T\ u_2^T\ ...\ u_p^T\right]$, and $u_k^T u_k = 1,\ k = 1, 2, ..., p$. The idea is to find the directions which maximizes the variance of the set $\{y_i\}$ that corresponds to the trace of the covariance matrix of $\{y_i\}$

$$A^* = \arg\max_A\ tr(C_y) \tag{3.32}$$

where

$$C_y = \frac{1}{N}\sum_{i=1}^{N}(y_i - \bar{y})(y_i - \bar{y})^T \tag{3.33}$$

and

$$\bar{y} = \frac{1}{N}\sum_{i=1}^{N} x_i \tag{3.34}$$

Let $C_x$ be the covariance matrix of the dataset $\{x_i\}$. It is easy to show that $tr\left(C_y\right) = tr(A^T C_x A)$. The goal is to maximize the variance, but to do this the focus should be limited to unit vectors as the maximization should be constrained (because if no constraint is chosen, a very large $A$ can be used). Therefore, to maximize the variance additional constraints should be added, that is, the only acceptable solutions should satisfy $A_k^T A_k = 1$. Now, we have a constrained optimization to resolve. A function $f(A_k) = A_k^T C_x A_k$ to maximize, along with an equality function $g(A_k) = c$, where $g(A_k) = A_k^T A_k$ and $c = 1$.

Therefore, the Lagrange multiplier $\lambda_k$ can be added to the equation, which would yield to the new objective function

$$L(A_k, \lambda)_{\mathrm{k}} = f(A_k) - \lambda_k(g(A_k) - c) = A_k^T C_x A_k - \lambda_k(A_k^T A_k - 1) \quad (3.35)$$

Now, the constrained optimization problem can be solved through unconstrained optimization of $L(A_k,\lambda_k)$. In order to find a global maximum of the optimization problem, the Kuhn-Tucker conditions can be used. These Kuhn-Tucker conditions state that:

- Any $A_k^*$ is a global minimum if and only if $A_k^*$ is feasible and there exist $\lambda_k^*, k = 1, \dots, p$ such that
  - $\nabla_{A_k} L(A_k^*, \lambda_k^*) = 0 \; \forall k$
  - $\lambda_k^* \geq 0, \forall k$
  - $\lambda_k^*(g(A_k) - c) = 0, \forall k$

In the PCA case the Kuhn-Tucker conditions to solve the optimization yields

$$\nabla_{A_k} L(A_k, \lambda_k) = 0 \Rightarrow \frac{\partial L}{\partial A_k} = 2C_x A_k - 2\lambda_k A_k = 0 \Rightarrow C_x A_k = \lambda_k A_k \quad (3.36)$$

$$\lambda_j \geq 0, \forall j \quad (3.37)$$

$$\lambda_k(g(A_k) - c) = 0 \quad (3.38)$$

Thus, $A_k$ is the eigenvector of the covariance $C_x$, which would satisfy the Kuhn-Tucker criteria. Therefore, the new space that gives a better insight of the data content and linearly separate them, is the space spanned by the eigenvectors of the covariance matrix. Most of the data variability lies in the eigenvectors that correspond to the largest eigenvalues.

Consequently, the data can be presented as

$$x_i = \sum_{k=1}^{p} (x_i^T A_k) A_k \tag{3.39}$$

which can be approximated to

$$x_i = \sum_{k=1}^{M} (x_i^T A_k) A_k \tag{3.40}$$

where $M < p$. In this case, the number of eigenvectors is reduced and by consequence, the dimensions in which the data is represented are reduced.

To summarize the procedure, the following steps can be used to apply the PCA on the fault detection:

*Step 1*

The raw dataset describing the dynamics of the system should be at a first stage normalized, i.e., subtract the mean and divide each data point by the standard deviation. The mean and the standard deviation are calculated respectively according to the following formulas

$$\bar{x} = \frac{\sum_{k=1}^{N} x_k}{N} \tag{3.41}$$

$$s^2 = \frac{\sum_{k=1}^{N} (x_k - \bar{x})^2}{N - 1} \tag{3.42}$$

where *N* represents the number of observations.

The reason behind the normalization of the dataset is to not bias the result of the procedure since at its origin the PCA seeks to maximize the variance, and if no normalization has been used, the variable having the maximum variance in the original

data will be dominant, and the PCA will perform poorly.

*Step 2*

The second step is to find the covariance matrix, which represents the correlation between the variables of the normalized dataset. The stronger the correlation, the higher the values in the covariance matrix.

$$C = \begin{pmatrix} cov(x,x) & cov(x,y) & cov(x,z) \\ cov(y,x) & cov(y,y) & cov(y,z) \\ cov(z,x) & cov(z,y) & cov(z,z) \end{pmatrix} = (N-1)^{-1} X^T X \qquad (3.43)$$

where $cov(x,y) = \frac{\sum_{k=1}^{N}(x_k - \bar{x})(y_k - \bar{y})}{N-1}$ and $X = [x_1 x_2 \dots x_N]^T$ represents the dataset matrix.

*Step 3*

The eigenvalues and eigenvectors of the covariance matrix are calculated according to the Equation (3.44)

$$CA = \lambda A \qquad (3.44)$$

where $A$ and $\lambda$ represent the eigenvectors and eigenvalues of the covariance matrix. In fact, the new dimension that the PCA seeks is the one spanned by the eigenvectors of the covariance matrix.

*Step 4*

Representing the spread of the data in each corresponding eigenvector direction, the eigenvalues are the keys to determine the reduced size and which of the eigenvectors should be kept. The higher the eigenvalue value, the more important the corresponding eigenvector. Therefore, sorting the eigenvalues and their corresponding eigenvectors forms the next step in the formulation of the principal components. The choice of the most critical eigenvectors is challenging considering that it will affect the residual space or what is

considered as the disturbance on the data. A bad choice of the number of eigenvectors will affect the performance of the procedure. If the number of eigenvectors is too high, a better representation of the raw dataset is guaranteed, but unnecessary information will be learned. On the other hand, if the number of the eigenvectors is too low, some critical data may get lost.

*Step 5*

To detect faults using the PCA procedure, two tools are usually considered, namely, the Hotelling's $T^2$ and $Q$ statistics (also called the squared prediction error (SPE)). $T^2$ and $Q$ represent the major variation and the random noise in the data respectively [87],[88]. Both techniques are based on statistical calculations that ensure a statistical limit on the projected data.

$T^2$ can be calculated as the sum of squares of a new process data vector $x_k$ as follows:

$$T^2 = x_k^T A \lambda_M^{-1} A^T x_k \tag{3.45}$$

where $\lambda_M$ is a squared matrix formed by the first $M$ rows and columns of $\lambda$.

The process is considered normal for a given significance level $\alpha$ if:

$$T^2 \leq T_\alpha^2 = \frac{(N^2-1)M}{N(\mathrm{N}-M)} F_\alpha(M, N-M) \tag{3.46}$$

where $F_\alpha(M, \mathrm{N}-M)$ is the critic value of the Fisher-Snedecor distribution with $N$ and $N - M$ degrees of freedom and $\alpha$ which takes values between 90% and 95% is the level of significance.

The scalar value $Q$ is a measurement of goodness of fit of the sample to the model and is directly associated with the noise and can be obtained at the $k^{th}$ sample as:

$$Q = r^T r \tag{3.47}$$

$$r = (I - AA^T)x_k \tag{3.48}$$

The upper limit of this statistic can be computed as

$$Q_\alpha = \theta_1 \left[ \frac{h_0 c_\alpha \sqrt{2\theta_2}}{\theta_1} + 1 + \frac{\theta_2 h_0 (h_0 - 1)}{\theta_1^2} \right]^{\frac{1}{h_0}} \tag{3.49}$$

$$\theta_k = \sum_{j=M+1}^{N} \lambda_j^i \qquad h_0 = 1 - \frac{2\theta_1 \theta_3}{3\theta_2^2} \tag{3.50}$$

where $c_\alpha$ is the value of the normal distribution with a $\alpha$-level of significance.

Both $T^2$ and $Q$ upper limits represent thresholds for the normal healthy data, above which the new state can be considered faulty. Steps 1 to 4 and the calculation of the upper limit of either $T^2$ or $Q$ are calculated off-line in the training phase. While during the on-line phase the tasks to be performed are summed in acquiring the new data point, scale it according to step one in the training procedure, calculate the $T^2$ or $Q$ accordingly and compare the obtained value with the limit set in the training. The $T^2$ and $Q$ statistical tests are mainly developed for linear systems. Based on the fact that the modular multilevel converter is a nonlinear system, the boundaries for both statistical techniques are not respected under normal operation. To remedy this issue, a user-defined threshold should be selected instead. The threshold is obtained based on observations of the healthy data points during the training phase. The fault detection algorithm using PCA is summarized in Figure 3.6 and the overall procedure is illustrated in Figure 3.7

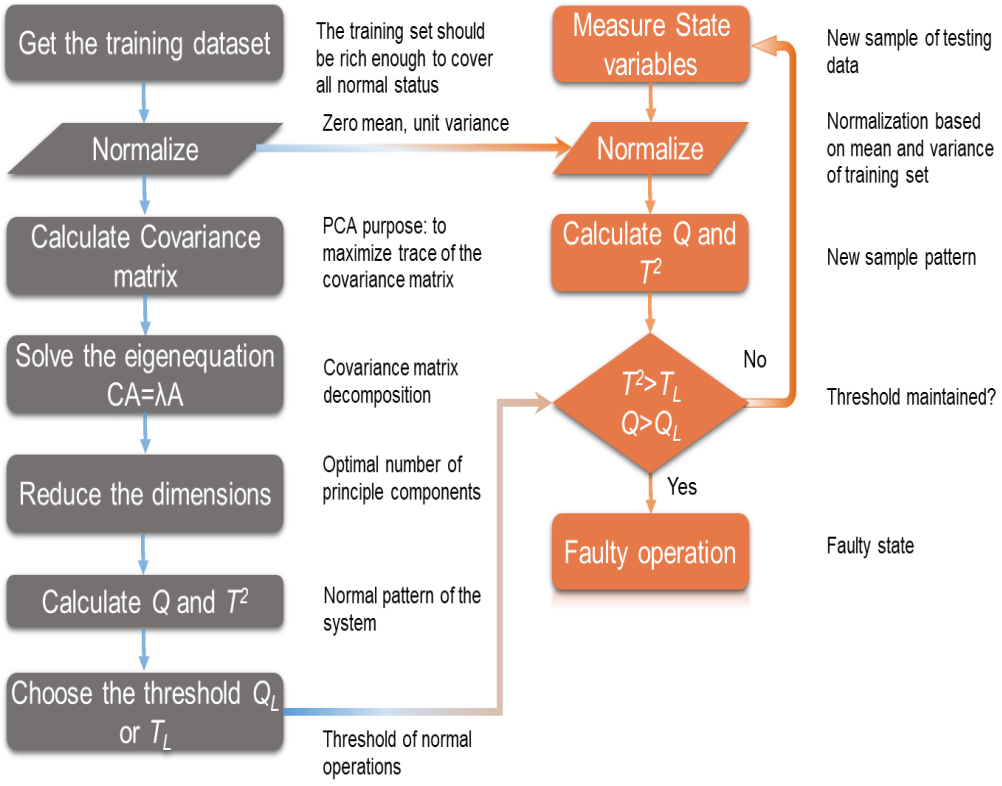


(a) (b)

Figure 3.6: Flowchart of fault detection procedure using PCA: (a) offline training, (b) online monitoring

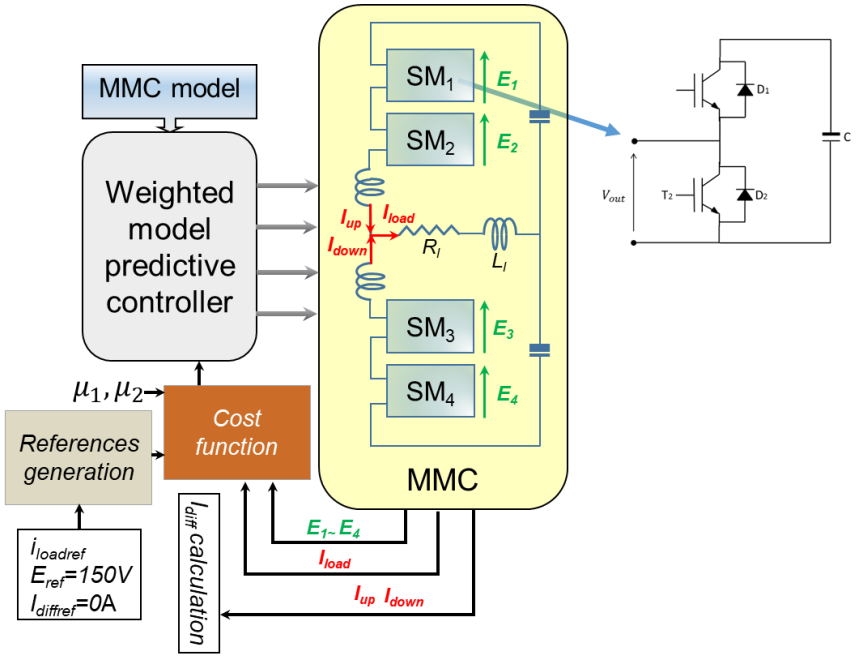


Figure 3.7: Control and fault detection in MMC using PCA technique

### *3.6.2 Kernel Principal Component Analysis*

The Modular Multilevel Converter is a nonlinear system, meaning that the variables are correlated nonlinearly, thus, weakening the performance of the PCA, which is designed to work with linear systems. To overcome the linearity issue, a nonlinear version of PCA can be introduced, which is the Kernel Principal Component Analysis (KPCA) [89]. The approach of KPCA takes advantage of the features presented by PCA and solves the linearity issue of the nonlinear systems [90]–[93]. The main idea of KPCA is to nonlinearly map the original data into a feature space, which is generally of higher dimension, before performing the PCA algorithm. Therefore, the mapped data can be viewed as linear in the

feature space [94], [95]. However, mapping each data point into a higher, possibly infinite, space would require additional calculation burden, which is a luxury that may not always be available, and it can be very costly in terms of computational time. To resolve this issue, KPCA offers a simple solution; the use of the kernel trick which allows the execution of PCA in the feature space without the explicit calculation of the projected data points. Therefore, instead of working with the projected data points in the feature space, the procedure makes all the necessary calculations in the original space using the kernel function since, in fact, the projections are not needed but instead the inner product, represented by the kernel function, between the data points. Consequently, the kernel trick allows the usage of the inner products in the feature space without the need to project the original dataset. Thus, the algorithms that use only the inner product can be performed implicitly in the feature space. The nonlinear mapping into the feature space and executing linear operations can be seen as performing nonlinear operations in the original space. Thus, performing PCA in the feature space is seen as performing nonlinear PCA in the original space, and consequently, the eigenvectors in the original space are no longer linear. Therefore, KPCA performs a nonlinear transformation into a much higher feature space $\mathcal{F}$ followed by a dimensionality reduction that allows performing a data compression while keeping the most valuable information. The choice of a convenient kernel function, which is a function that satisfies Mercer's theorem, is crucial to enhance the performance of the KPCA.

The most popular kernel functions used in the literature are:

- The polynomial kernel

$$k(x_i, x_j) = \langle x_i, x_j \rangle^d \tag{3.51}$$

- The Radial basis function (RBF)

$$k(x_i, x_j) = \exp\left(-\frac{\|x_i - x_j\|^2}{2\sigma^2}\right) \tag{3.52}$$

where $2\sigma^2$ represent the width of the Gaussian kernel.

- The sigmoid kernel

$$k(x_i, x_j) = \tanh(G\langle x_i, x_j \rangle + \theta) \tag{3.53}$$

for convenient gain *G* and threshold $\theta$.

Assuming that the function defined by $\Phi: R^N \rightarrow \mathcal{F}$ is the function used to map the data from the original space $R^N$ into the feature space $\mathcal{F}$, the covariance matrix in the feature space is:

$$C = 1/N \sum_{i=1}^{N} \phi(x_i)\phi^T(x_i) \tag{3.54}$$

where $\phi(x_i)$ is the $i^{th}$ component in the feature space, *N* is the data size and suppose that the projected points have zero mean and unity variance. Similar to the PCA case, the idea is to find the eigenvectors and eigenvalues of the covariance matrix in the feature space [96] and to do so one should resolve the following Equation (3.55)

$$Cv = \lambda v \tag{3.55}$$

where $\lambda$ and $v$ represent the eigenvalues and eigenvectors of the covariance matrix in the feature space, respectively. The $v$ corresponding to the largest $\lambda$ is considered the first

principal component (PC) and the one corresponding to the lowest eigenvalue is the last PC. Based on the equation of the covariance matrix in (3.54), Equation (3.55) can be rewritten as

$$\lambda v = \frac{1}{N}\left(\sum_{i=1}^{N} \phi(x_i)\phi^T(x_i)\right)v = \frac{1}{N}\sum_{i-1}^{N}\langle \phi(x_i), v\rangle \phi(x_i) \tag{3.56}$$

where $\langle x, y\rangle$ denotes the dot product between $x$ and $y$. Before proceeding, let's show that the inclusion of the inner product is justified in the Equation (3.56) and to do so let's show that $xx^T v = \langle x.\, v\rangle x^T$:

$$\begin{aligned}
(xx^T)v &= \begin{pmatrix} x_1x_1 & x_1x_2 & \cdots & x_1x_M \\ x_2x_1 & x_2x_2 & & x_2x_M \\ \vdots & & \ddots & \vdots \\ x_Mx_1 & x_Mx_2 & \cdots & x_Mx_M \end{pmatrix}\begin{pmatrix} v_1 \\ v_2 \\ \vdots \\ v_M \end{pmatrix} \\
&= \begin{pmatrix} x_1x_1v_1 + x_1x_2v_2 + \cdots + x_1x_Mv_M \\ x_2x_1v_1 + x_2x_2v_2 + \cdots + x_2x_Mv_M \\ \vdots \\ x_Mx_1v_1 + x_Mx_2v_2 + \cdots + x_Mx_Mv_M \end{pmatrix} \\
&= \begin{pmatrix} (x_1v_1 + x_2v_2 + \cdots + x_Mv_M)x_1 \\ (x_1v_1 + x_2v_2 + \cdots + x_Mv_M)x_2 \\ \vdots \\ (x_1v_1 + x_2v_2 + \cdots + x_Mv_M)x_M \end{pmatrix} \\
&= (x_1v_1 + x_2v_2 + \cdots + x_Mv_M)\begin{pmatrix} x_1 \\ x_2 \\ \vdots \\ x_M \end{pmatrix} = (x.\, v)x
\end{aligned} \tag{3.57}$$

Thus, the equality mentioned in (3.56) is valid, and this result implies that all eigenvectors that correspond to non-null eigenvalues lie in the span of the set $\phi(x_1), \phi(x_2), \ldots, \phi(x_N)$. By consequence, Equation (3.55) can be written as

$$\lambda\langle \phi(x_k), v\rangle = \langle \phi(x_k), Cv\rangle, \quad k = 1, 2, \ldots, N \tag{3.58}$$

In addition, the eigenvector $v$ can be written in function of $\phi(x)$

$$v = \sum_{i=1}^{N} \alpha_i \, \phi(x_i) \tag{3.59}$$

where $\alpha_i$ represent the weighting coefficients. Replacing $v$ in Equation (3.58) by its expression in Equation (3.59) yields

$$\lambda \sum_{i=1}^{N} \alpha_i \langle \phi(x_k), \phi(x_i) \rangle = \frac{1}{N} \sum_{i=1}^{N} \sum_{j=1}^{N} \alpha_i \, \langle \phi(x_k), \phi(x_j) \rangle \, \langle \phi(x_j), \phi(x_i) \rangle \tag{3.60}$$

for $k = 1 \dots N$

Determining the value of each mapped point in the feature space is both costly and inefficient. So, to avoid this drawback, the kernel trick can be used. Let us define the Gram kernel matrix $K$ as

$$[K]_{i,j} = \langle \phi(x_i), \phi(x_j) \rangle = K(x_i, x_j), \qquad i, j = 1 \dots N \tag{3.61}$$

Integrating the new concept into the Equation (3.60), yields

$$N \lambda K \alpha = K^2 \alpha \tag{3.62}$$

for nonzero $\lambda$ and as $K$ is a positive definite matrix, Equation (3.62) can be rewritten in the form

$$N \lambda \alpha = K \alpha \tag{3.63}$$

Therefore, instead of dealing with the covariance matrix $C$ directly, the final problem is to diagonalize the Gram kernel matrix $K$.

Suppose the eigenvalues of the matrix $K$ are denoted by $\lambda_1 > \lambda_2 > \cdots > \lambda_N$, and $\alpha_1, \alpha_2, \dots, \alpha_N$ their corresponding eigenvectors. Each eigenvector needs to be normalized in the feature space as required by the PCA.

Therefore, the eigenvectors should satisfy

$$\langle v_k, v_k \rangle = 1, \qquad k = 1, .., p \tag{3.64}$$

Given that the number of retained eigenvalues after applying the PCA in the feature space is $p$. This leads to

$$\begin{gathered} \langle \sum_{i=1}^{N} \alpha_i^k \phi(x_i) , \sum_{j=1}^{N} \alpha_j^k \phi(x_j) \rangle = 1 \Rightarrow \sum_{i=1}^{N} \sum_{j=1}^{N} \alpha_i^k \alpha_j^k K_{ij} = 1 \\ \Rightarrow \langle \alpha_k , K\alpha_k \rangle = 1 \Rightarrow \lambda_k \langle \alpha_k, \alpha_k \rangle = 1 \end{gathered} \tag{3.65}$$

which means that each $\alpha_k$ should be divided by $\sqrt{N\lambda_k}$.

As in PCA, the data points in KPCA are projected onto the eigenvectors $V_k$ of the covariance matrix

$$\langle v_k , \phi(x) \rangle = \sum_{i=1}^{N} \alpha_i^k \langle \phi(x_i), \phi(x) \rangle = \sum_{i=1}^{N} \alpha_i^k K(x_i, x) \tag{3.66}$$

Equation (3.66) is valid when the projection is made over the whole range of eigenvectors. However, if a linear relationship can be achieved in the feature space then projecting on the first *p* eigenvectors is sufficient to present the data accurately. Hence the needed eigenvectors and eigenvalues are limited to the first *p* largest ones, and the projected principal component can be calculated as

$$\langle v_k , \phi(x) \rangle = \sum_{i=1}^{p} \alpha_i^k \langle \phi(x_i), \phi(x) \rangle = \sum_{i=1}^{p} \alpha_i^k K(x_i, x) \tag{3.67}$$

The mapped data in the feature space were supposed to be centered when formulating the KPCA procedure [97]–[100]. However, this might not be guaranteed in most cases even if the original dataset was centered in the original space.

In addition since, $\phi(x)$ is not known explicitly, the centering procedure shall be done by centering the kernel matrix instead [81], [101]. So, suppose the centered points in the feature space is defined as

$$\tilde{\phi}(x_k) = \phi(x_k) - \frac{1}{N}\sum_{i=1}^{N}\phi(x_i) \tag{3.68}$$

Then, the centered kernel matrix in the feature space would have the form

$$\begin{aligned}\widetilde{K}_{ij} &= \langle\tilde{\phi}(x_i), \tilde{\phi}(x_j)\rangle \\ &= \langle\phi(x_i) - \frac{1}{N}\sum_{l=1}^{N}\phi(x_l)\,, \phi(x_j) - \frac{1}{N}\sum_{n=1}^{N}\phi(x_n)\rangle \\ &= K_{ij} - \frac{1}{N}\sum_{l=1}^{N}K_{ik} - \frac{1}{N}\sum_{n=1}^{N}K_{jn} + \frac{1}{N^2}\sum_{l=1}^{N}\sum_{n=1}^{N}K_{nl}\end{aligned} \tag{3.69}$$

This yields that

$$\widetilde{K} = K - 1_N K - K 1_N + 1_N K 1_N \tag{3.70}$$

where $1_N = \frac{1}{N}\begin{bmatrix}1 & \cdots & 1\\ \vdots & \ddots & \vdots\\ 1 & \cdots & 1\end{bmatrix}$ represent an $N \times N$ matrix.

The goal is to find matching parameters (the value of *p* that determines the most significant eigenvectors, and the kernel parameters) that would, to the best extent, describe the pattern of the training set.

Now, to evaluate the fitness of a new data point to the pattern set by the training phase, assume that the new *m*-dimensional vector of measurable variables is denoted by $x_{test} = [x_1\ x_2\ \ldots\ x_m]$. The new set is normalized, with respect to the mean and standard deviation used in the training phase, prior to the calculation of the kernel matrix.

The formulation of the new kernel matrix is done by evaluating the test point against each training point

$$K_{test} = [k(x_{test}, x_{train1})\ k(x_{test}, x_{train2}) \dots k(x_{test}, x_{trainN})] \tag{3.71}$$

The new kernel needs to be centered in the feature space with respect to the training set, and it is done by

$$\widetilde{K}_{test} = K_{test} - \frac{1}{N}\underbrace{(1\ 1 \dots 1)}_{(1\times N)} K - K_{test} 1_N + \frac{1}{N}\underbrace{(1\ 1 \dots 1)}_{(1\times N)} K 1_N \tag{3.72}$$

On the other hand, the kernel function between each test point and itself can be calculated as $K_e = k(x_{test}, x_{test})$ and it is centered through

$$\widetilde{K}_e = K_e - \frac{2}{N} K_{test} \underbrace{(1\ 1 \dots 1)}_{(N\times 1)}^T + \frac{1}{N}\underbrace{(1\ 1 \dots 1)}_{(1\times N)} K \underbrace{(1\ 1 \dots 1)}_{(N\times 1)}^T \tag{3.73}$$

Taking into consideration that if the data points are projected into all the eigenvectors, the data is preserved and the PCA is in this case just a change of coordinates. Performing PCA in the feature space means that only a few most significant eigenvalues are considered for the data projection. The resulting error from both projections can be evaluated, and a threshold can be elaborated based on the healthy data during the training phase.

The squared error between data projection on the full eigenvector space and principal component space can be evaluated as [102]

$$e_{proj} = \|e\|^2 = \left\|X^{proj}\right\|^2 - \left\|X^{proj(p)}\right\|^2 \tag{3.74}$$

The evaluation of the projection on the *p* principal component can be evaluated using the Equation (3.67) such that

$$X^{proj(p)} = \sum_{i=1}^{p} \alpha_i^k \langle \tilde{\phi}(x_i), \tilde{\phi}(x) \rangle = \sum_{i=1}^{p} \alpha_i^k \tilde{K}(x_i, x) \tag{3.75}$$

whereas, the projection onto the whole eigenvectors space can add more computational load. To mitigate this, one should consider that the data in the feature space are centered, which means that the new basis is a pure rotation of the old basis and no translation is involved. Besides, only the squared distance between the data point and the origin is needed. Consequently, the data projection on the whole eigenvector space can be evaluated

$$\left\| X^{proj} \right\|^2 = \langle \tilde{\phi}(x), \tilde{\phi}(x) \rangle \tag{3.76}$$

which is, in fact, the kernel function calculated above and denoted as $\tilde{K}_e$.

Therefore, it is possible to construct a threshold between the projection of the data points into the whole eigenvector space, and their projection into space spanned by the principal components in the feature space. This threshold is established based on the maximum allowable error calculated from the observations errors during the training phase and taking into account the effect of possible disturbances. Similarly, during the online phase, the error between the two projections is monitored and compared with the established threshold. A fault is detected if the projection errors of the new data points exceed the threshold for a specified period.

To recapitulate, KPCA can be applied to the system by executing selected actions during the off-line phase, or what is called the training phase, and others during the online operations, or what is called the monitoring phase. The procedure to perform the KPCA algorithm is illustrated in Figure 3.8, and the tuning of the KPCA parameters can be performed using the steps described in the flowchart illustrated in Figure 3.9.

The steps to formulate the error contours that delimit the healthy operation and the monitoring process using KPCA are described in the next subsection.

*3.6.2.1 Off-line training*

Step 1.

The raw dataset should be at a first stage normalized, and the kernel matrix should be calculated $K(x_i, x_j)$

Step 2.

Perform the centering procedure of the image according to Equation (3.70)

$$\widetilde{K} = K - 1_N K - K 1_N + 1_N K 1_N$$

Step 3.

Solve the eigenequation $N\lambda\alpha = \widetilde{K}\alpha$ and normalize the $\alpha_k$, by dividing each $\alpha_k$ by $\sqrt{N\lambda_k}$.

Step 4.

Choose the number of principal components based on user-defined criteria (e.g. $\frac{\sum\lambda_{retained}}{\sum\lambda_k} * 100 \geq 80\%$).

Step 5.

Calculate the threshold of the normal data by calculating the error between the projection of the data points into the whole eigenvector space and their projection into the principal component space.

*3.6.2.2 On-line training*

Step 1.

Acquire new data point and scale it using the mean and standard deviation used in step 1 in the training phase.

Step 2.

Calculate the kernel matrix $K_{test}$ between the new data point and the all the training points then perform the centering procedure with respect to the training set.

*Step 3.*

Calculate the kernel matrix $K_e$ between the new data point and itself then perform the centering procedure.

*Step 4.*

Calculate the projection error of the new data point on the whole eigenvector space and its projection on the principal components space.

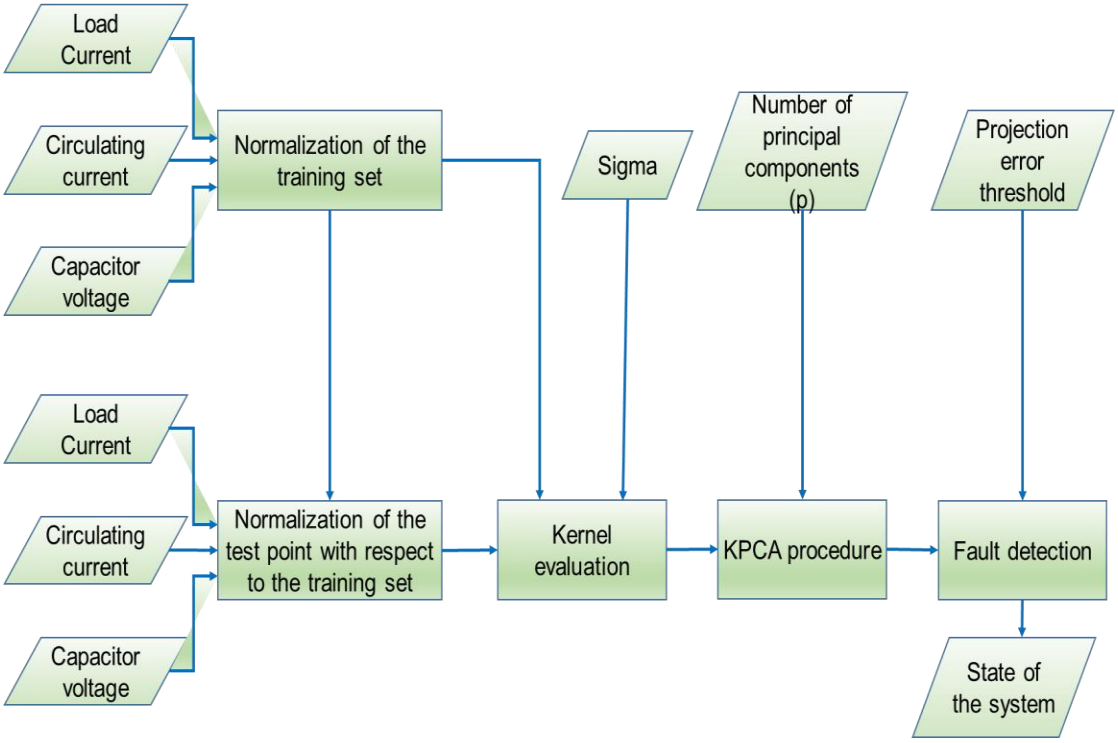


Figure 3.8: Data processing for fault detection using KPCA algorithm

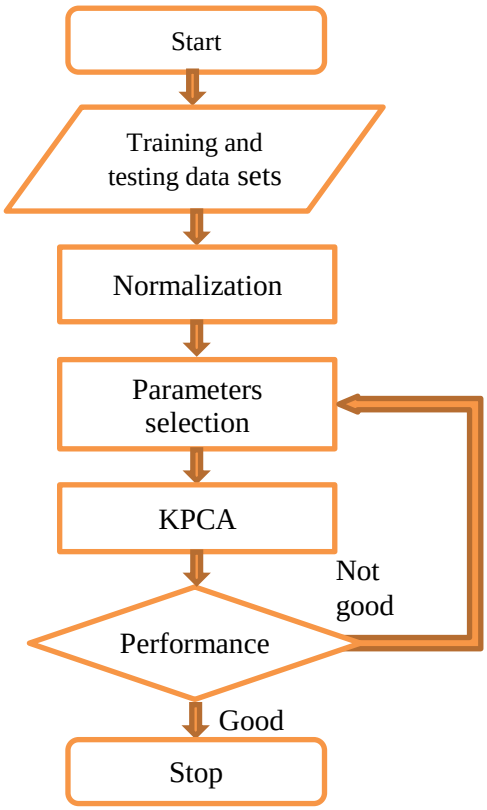


Figure 3.9: Flowchart of KPCA training

## 3.7 Fault Localization

As mentioned previously, the fault localization using PCA with a nonlinear system such as the MMC, which incorporates a high number of redundant submodules connected in series, is somewhat challenging and the simulation results revealed high rate of misclassifications (over 70%) of the fault locations, and that is the reason behind the use of, solely, the KPCA for fault identification. Three approaches were considered in the fault identification using the KPCA that are detailed in the below subsections.

### *3.7.1 Approach 1*

The set of variables considered in this approach are the capacitor voltages of different cells, the circulating current, and the load current. Note that these parameters are already available for control purposes in both MPC and voltage-balancing controls. Other variables may be considered such as the output voltage, which is used in the literature to evaluate the faults and their locations. However, this would require additional sensors, and thus it increases the cost of the converter, and it is not a preferable practice in the industry since it contains high-frequency components. As stated before, the fault dynamics in MMC affect all the state variables and create a new pattern that can be identified uniquely for that specific open circuit fault. Therefore, the proposed technique for fault isolation in this approach is to learn the different fault scenarios related to different power switches. Consequently, in the case of four cells MMC, eight power switches are considered, and eight fault scenarios have to be learned. The concept of the fault localization is to learn the fault scenarios related to different switches at a given sampling time for a given arm current direction, and a given load, which would lead to eight projection error thresholds and thus eight fault classes are constructed. In the monitoring phase the projection error of the new faulty data points is calculated. Due to the transient phase in the system dynamics after the fault occurrence, the KPCA is susceptible to make some misclassifications. One way to mitigate this drawback is to calculate the accumulative projection errors over a specific period and the final fault location is then identified based on the accumulated error. Consequently, the KPCA module which results in minimum error corresponds to the faulty switch. The proposed procedure to perform the fault localization using the full state variables is as illustrated in Figure 3.10, where the KPCA models are created using the data

generated by applying open circuit faults to each switch in the converter. Considering that the number of submodules in MMC is 2*N*, the generated number of KPCA models is 4*N*. The residual generated in the output of each KPCA model corresponds to the instantaneous projection error, and this residual is then accumulated over a period of time, and the fault localization is finally based on the residual generating the minimum error.

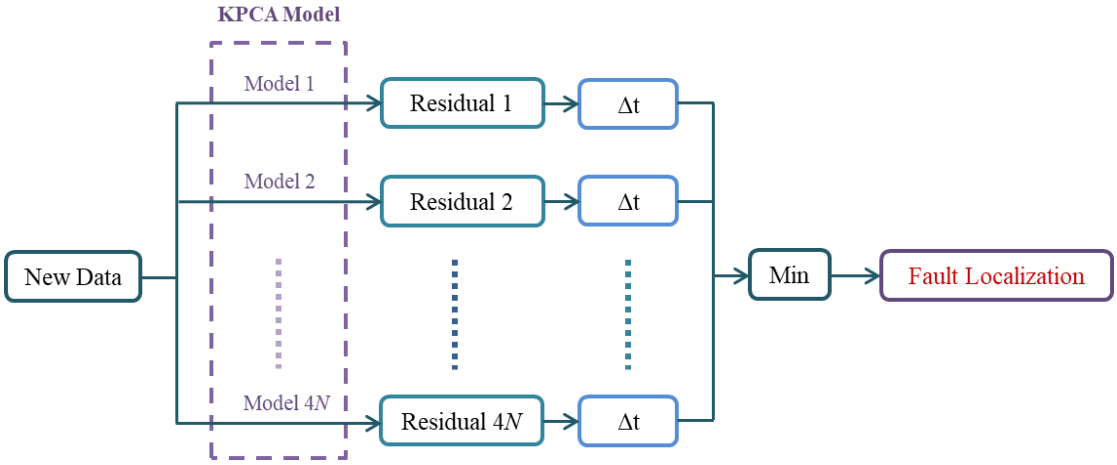


Figure 3.10: Fault localization procedure using full state KPCA

### *3.7.2 Approach 2*

In this subsection, the same principle adopted in the first approach is used to establish the fault localization with one single modification; Instead of using the state variables directly as inputs to the localization procedure, data preprocessing is performed before the analysis using KPCA. Hence, instead of using the capacitor voltages along with the circulating and load currents, the focus is maintained only on the capacitor voltages since the fault impact is more distinguishable using the capacitor voltages behavior as illustrated in the elaboration of the system dynamics under open circuit faults. The idea behind the data preprocessing is to enlarge the error when the corresponding switch is healthy. Based on the dynamic behavior under faulty states, the new variables used as inputs to the KPCA module include the corresponding capacitor voltage $E_k$, the sum of the capacitor voltages belonging to the same arm $\sum_{arm} E_k$, which would increase rapidly if the faulty switch is located within the same arm and it helps to differentiate between the faults occurring in the upper and lower switches since the fault pattern is different in each case, which reflects on the voltage sum. Also, the difference between the upper and lower arm capacitor voltages is used as an indication about the faulty arm $\sum_{uparm} E_k - \sum_{lowarm} E_k$, taking into account that that the capacitor voltage increase in the faulty cell creates an unbalance between the two arms that is in favor of the arm containing the faulty power switch. Besides, the cubic difference between the corresponding capacitor voltage and its reference signal is also used $\left(E_k - E_{ref}\right)^3$, which represents a direct indication about the status of the corresponding cells switches considering that this difference should increase substantially when the corresponding cell contains the faulty switch. The cubic power would accentuate

the rate of voltage difference increase for the faulty cell compared to other cells with keeping the difference sign. The last two inputs include the Euclidean distance of the corresponding capacitor voltage to the remaining capacitor voltages $\sqrt{\sum_{k=1,k\neq j}^{2N}\left(E_j - E_k\right)^2}$ and the sum of the normalized capacitor voltage with respect to the other ones $\sum_{k=1,k\neq j}^{2N}\frac{E_j}{E_k}$. Note that this input change enhances the segregation between the projection errors corresponding to different cells, however, it does not guarantee the proper localization within the cell and misclassifications between the upper and lower power switches that belongs to the same submodule can occur. Nevertheless, the proper localization of the faulty cell is acceptable since the fault tolerant control will bypass the whole submodule anyway, once the localization is achieved and later on the proper localization within the faulty cell can be performed.

### *3.7.3 Approach 3*

In this approach, a partial KPCA, which is a KPCA performed on a reduced number of input parameters, is used to perform the fault localization. The idea behind the use of partial KPCA is that removing a state variable from the calculations of the projected error reduces the latter by a quantity that is proportional to the state variable effect i.e. if the removed variable is healthy the error reduction should be small and contrarily if the removed variable is faulty then a substantial reduction can be seen. The procedure of the partial KPCA is to construct a set of 2*N* KPCA modules, where *N* represents the number of submodules in each arm. Each of these modules contains *m*-1 inputs such that each of the state variable, the capacitor voltage, in this case, exists only in *m*-1 KPCA modules. Note that the number of submodules considered in this case 2*N* is equal to the number of

state variables *m*, used as input to the KPCA algorithm. The resultant output of the module that does not use the input corresponding to the faulty cell would result in the lowest error. The advantage of this approach is that it does not require to train the modules on the faulty behavior and it is sufficient to train the KPCA on the healthy data. However, the fault location can only be traced back to the submodule level, and exact faulty switch cannot be identified. The proposed algorithm for fault localization using the partial KPCA is illustrated in Figure 3.11, and the overall process is illustrated in Figure 3.12

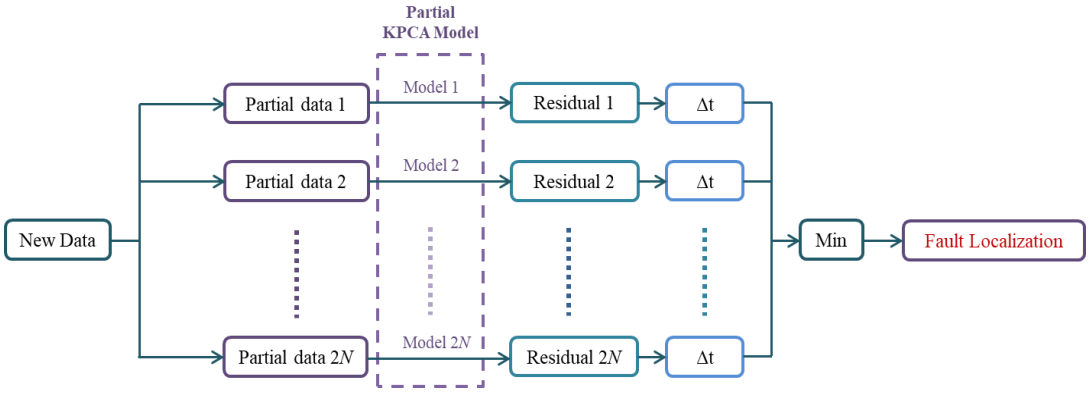


Figure 3.11: Fault localization procedure using Partial KPCA

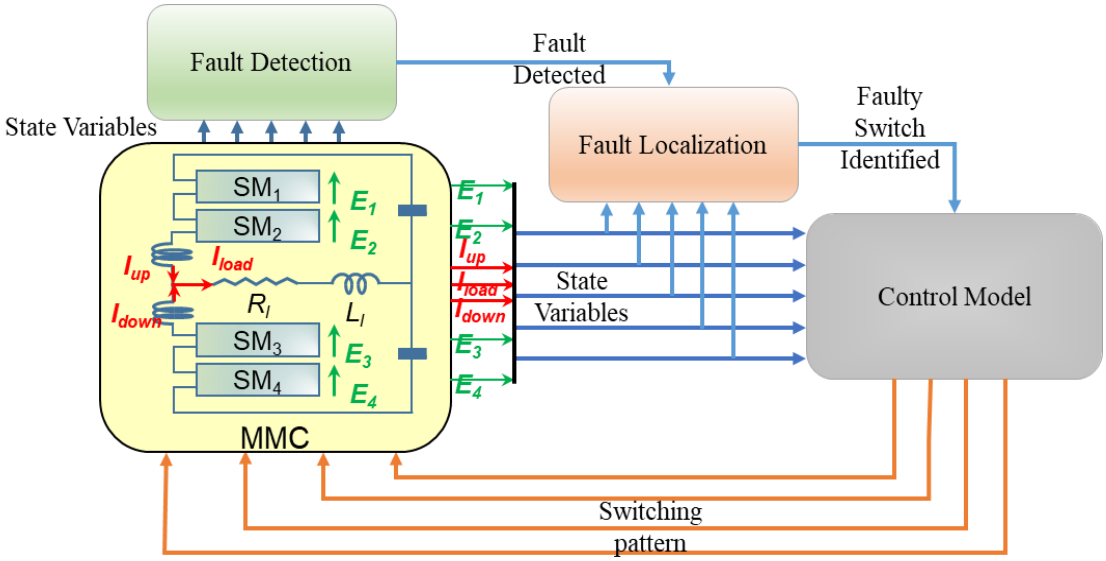


Figure 3.12: Overall fault detection and localization procedure

# CHAPTER 4: SIMULATION RESULTS AND DISCUSSION

In this section, the focus is to validate the proposed methodology using two converters with different sizes, ratings and using two different control approaches. The simulation results of the two converters under normal and faulty behavior are presented at first stage followed by the presentation of the fault detection results using the PCA and KPCA under various working conditions, and finally, the fault localization results using the different approaches are tackled.

## 4.1 Model Predictive Control under Normal and Faulty States

The simulations of the first adopted technique, model predictive control, are carried using Matlab/Simulink. The considered MMC is a four cells converter, and the used parameters are listed in Table 4.1 below [38]

Table 4.1: Simulation parameters for the MMC under predictive control

| Parameters | Values |
|---|---|
| Load resistor $R_L$ | 19 Ω |
| Load inductor $L_L$ | 50 mH |
| Arm resistor $R$ | 0 Ω |
| Arm inductor $L$ | 1 mH |
| Cells capacitor $C$ | 1000 μF |
| Fundamental frequency $f$ | 50 Hz |
| Sampling frequency $F_s$ | 10 KHz |
| Input voltage $V_{dc}$ | 300 V |
| Number of submodules per arm $N$ | 2 |
| Reference load current $I_{loadref}$ | 3 A |

Note that the adopted technique uses weighting factors on the circulating current and the load current during the calculation of the cost function, which should be tuned in order to achieve better performance. The used weighting factors during the simulation are $\lambda=10\times\beta=2\times10^{-2}$. The simulation results under normal operating conditions are illustrated in Figure 4.1. As it can be seen, after a transient that occurs in the starting of the converter after which all the capacitors are charged, and the system is stabilized, the tracking of the load current is achieved with minimal error, the circulating current is kept in low values around zero, and the capacitor voltages are oscillating around their reference value $\frac{V_{dc}}{2}$ with a small error margin. However, the introduction of an open circuit fault in any of the power

switches disrupts the normal behavior of the converter as illustrated in Figure 4.2, which shows the system behavior when an open circuit fault is injected in the upper switch $T_1$ of cell 1. The Figures 4.2 (a)-(e) represent the capacitor voltage, the upper and lower arms currents, the circulating current, the reference and actual load currents, and the output voltage variations under normal and faulty conditions, respectively. As it can be seen all the parameters have diverged from their initial, stable states as a result of the fault occurrence. As shown in Figure 4.2 (a), the fault effect is not only limited to the faulty cell but it propagates to the other cells via the dynamics of the system and the control effects (upon the fault occurrence, the controller tries to bring the system back to stability by changing the switching pattern). The fault propagation in this case resulted in total unbalance between the upper and lower arms' currents (Figure 4.2 (b)), a very high circulating current with peaks over 20A while the rated load current is just 3A and the output current and voltage were zeroed after the fault occurrence by 4.2s.

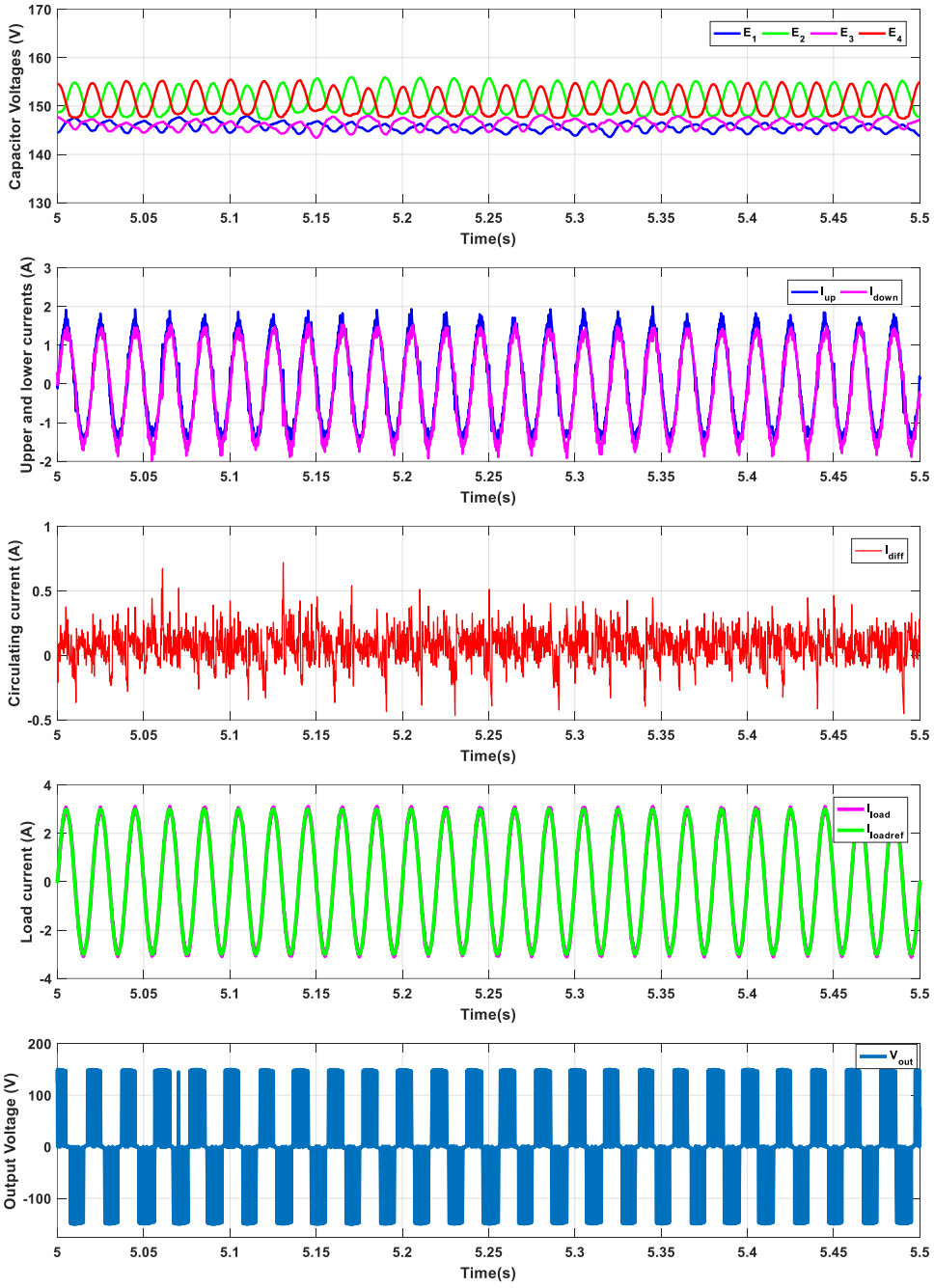


Figure 4.1: Waveforms of healthy state variables of the MMC under MPC control

Note that upon the fault occurrence, the system goes into a transient period where the controller tries to achieve the needed balance by adjusting the switching signals and considering that the fault is just a disturbance, however, with the fault expansion, the controller cannot handle the system and this leads eventually to total instability.

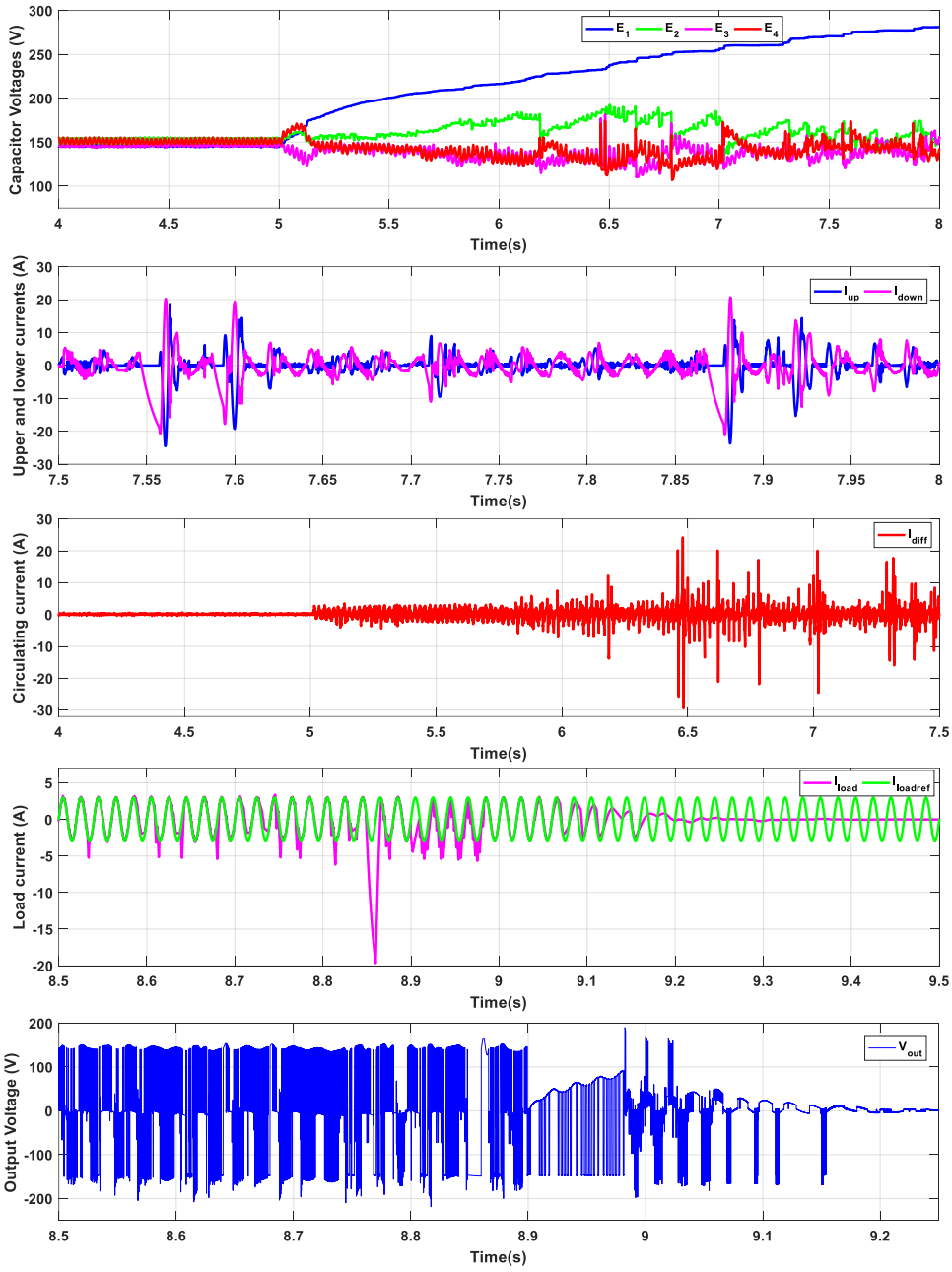


Figure 4.2: Waveforms of faulty state variables of the MMC under MPC control

## 4.2 Pulse Width Modulation Control under Normal and Faulty States

In this section, an eight cells MMC is considered. The converter is controlled through a PWM-based voltage-balancing controller that uses a phase shifted carrier. The controller design and properties are discussed in Section 3.4, and the used simulation parameters along with the gain values of the PI controllers are as depicted in Table 4.2

Table 4.2: Simulation parameters for the MMC under voltage-balancing control

| Parameters | Values |
|---|---|
| Load resistor $R_L$ | 26 Ω |
| Load inductor $L_L$ | 40 mH |
| Arm resistor $R$ | 0 Ω |
| Arm inductor $L$ | 3 mH |
| Cells capacitor $C$ | 1900 μF |
| Fundamental frequency $f$ | 50 Hz |
| Carrier frequency $F_c$ | 2 KHz |
| Input voltage $V_{dc}$ | 9 kV |
| Number of submodules per arm $N$ | 4 |
| Reference load voltage $V_{outref}$ | 4.5 kV |
| Proportional gain $K_1$ | 0.5 |
| Integral gain $K_2$ | 150 |
| Proportional gain $K_3$ | 1.5 |
| Integral gain $K_4$ | 150 |
| Proportional gain $K_5$ | 0.35 |

Similarly to the case of MPC, the simulation waveforms shown in Figure 4.3 show that the voltage-balancing controller is capable of effectively tracking the voltage reference signal. Although this reference signal is tracked using an open loop control, the usage of PI controller to control the average and individual capacitor voltage along with circulating current reduction can achieve great tracking performance.

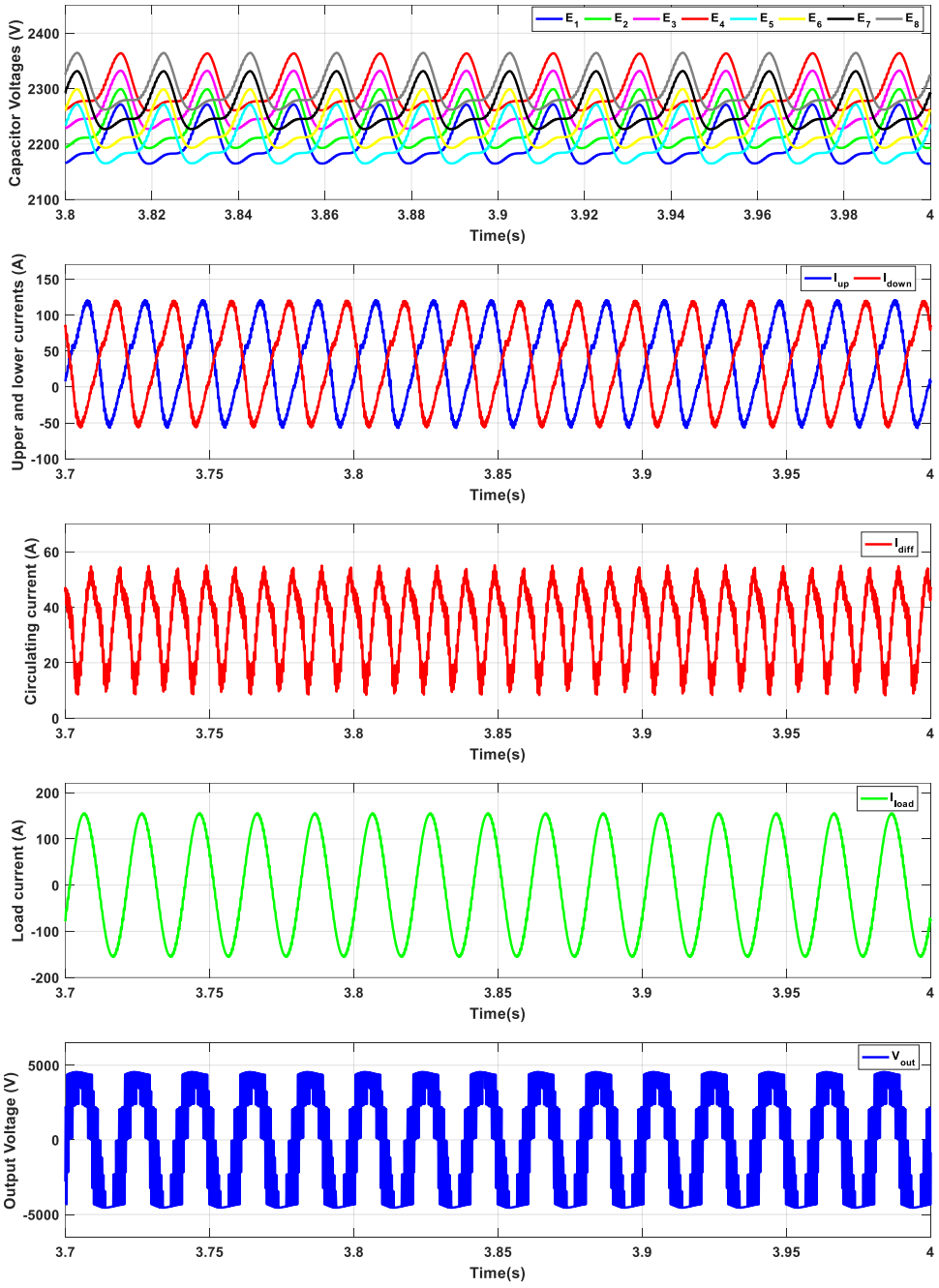


Figure 4.3: Waveforms of healthy state variables of the MMC under voltage-balancing control

In addition, it can be noticed that the divergence of the capacitor voltages in case of open circuit faults presented in Figure 4.4, shows shorter transient when compared to the MPC control case, which is an indicator of the low involvement of the controller in this case when a major fault occurs to the system. This low involvement is due to the existence of the open loop control in the case of the voltage-balancing control.

According to the presented simulations, the impact of an open circuit fault may deteriorate the waveforms of all the parameters and may result in components failure and even total shutdown if not detected and isolated in the earliest. In the next subsections, the fault detection using PCA and KPCA in both configurations is discussed, followed by fault localization using different approaches.

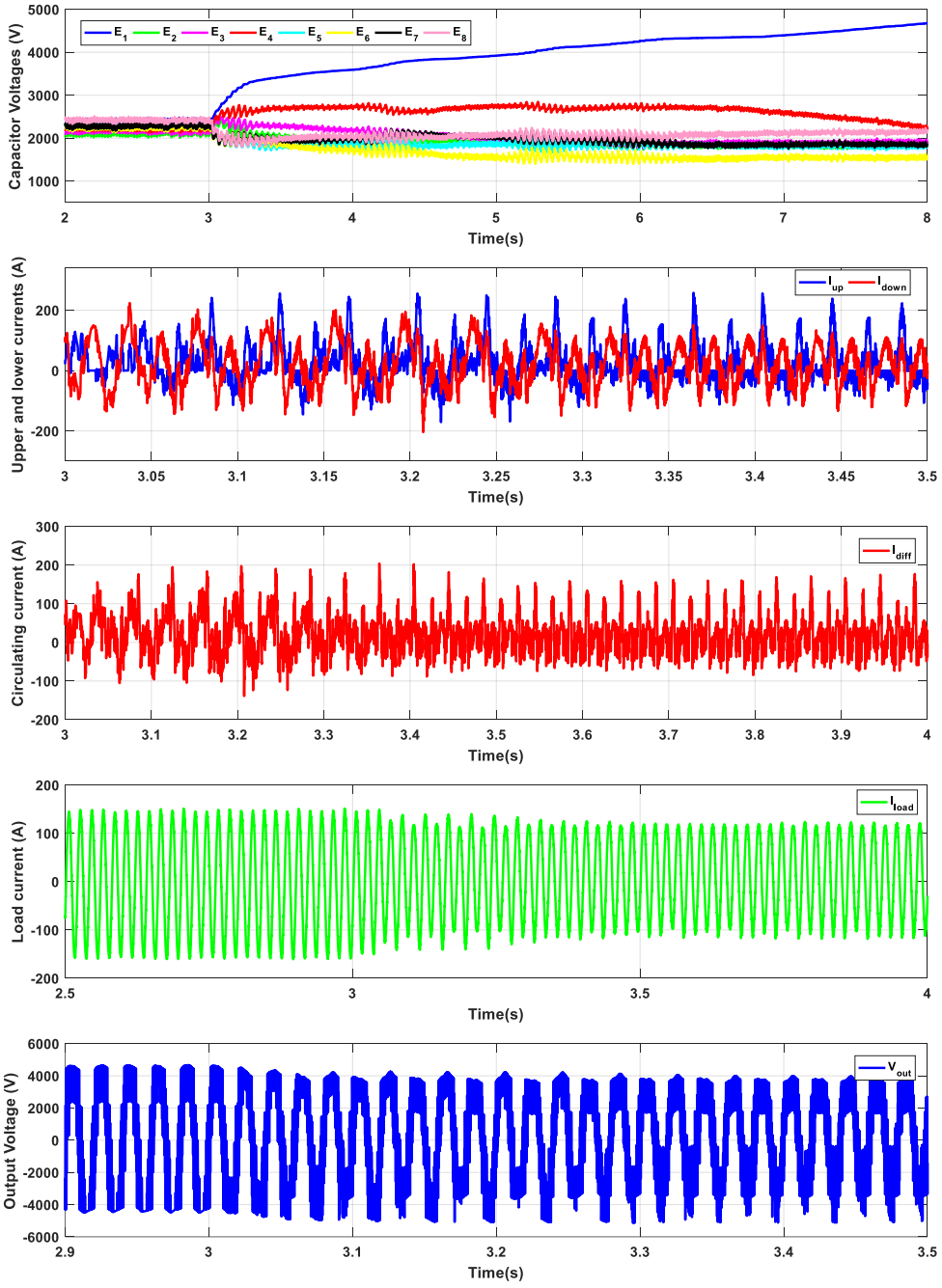


Figure 4.4: Waveforms of faulty state variables of the MMC under voltage-balancing control

## 4.3 Open Circuit Fault Detection

The performance of the two adopted fault detection techniques is tested using the two MMC configurations and simulation results are illustrated in the following subsections.

### *4.3.1 Fault Detection using PCA*

The circulating current, capacitor voltages and load current are chosen to be the state variables for the PCA monitoring procedure. Two hundred observations, which represent one full cycle, are used to train the PCA in the off-line phase. On the other hand, during the on-line monitoring phase, the fault detection using PCA requires the use of one of the two statistical tests $T^2$ and $Q$ to evaluate the new data points in comparison to the healthy ones. Since PCA makes a dimensional reduction, it is essential to choose the eigenvalues that represent the original dataset to the best extent while removing the effect of noises and disturbances. For the case of PCA with the MPC control, where six state variables are presented and as shown in Figure 4.5, three of the six eigenvalues can explain 95% of the original data, which would be sufficient to represent the data with adequate accuracy. Thus, the data is projected on the three eigenvectors corresponding to the three largest eigenvalues.

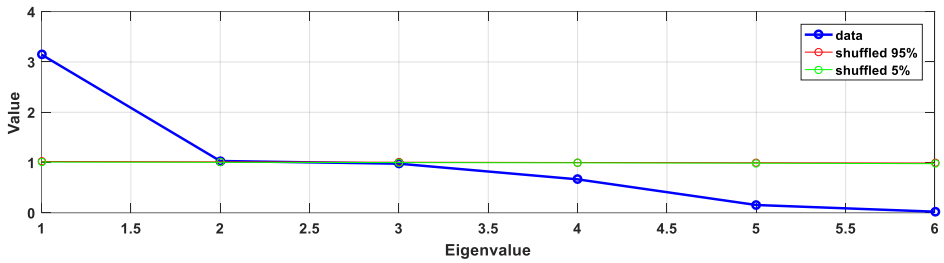


Figure 4.5: Eigenvalues of the six state variables using MPC control and their importance

Another important parameter to be considered in PCA is the threshold seperating the healthy from the faulty cases. As shown in Figure 4.6, the $T^2$ and $Q$ tests diverge rapidly when the fault occurs, which represent an adequate indicator of the faulty states. The threshold that separates the normal behavior from the faulty one is user-defined and since the load of the MMC may vary over time the values of the statistical tests will also vary accordingly. However, using the fact that the divergence of both tests is rapid, the threshold can be set at high values that assure fast fault detection and proper operation in the ordinary case. In the simulated case, the thresholds of the $T^2$ and $Q$ are set to 100 and 20 respectively, which is much higher than the normal operation variations. Nevertheless, these thresholds guarantee false alarm free operation and fast detection in case of faulty state when PCA control is considered. Consequently, the variation of the reference current did not affect the fault detection time and both have detected the fault after 13$ms$ from its occurrence. Note that both $T^2$ and $Q$ are considered in the simulations, and the fault detection is based on the fastest test to detect the anomaly, which in this case represented by the $T^2$.

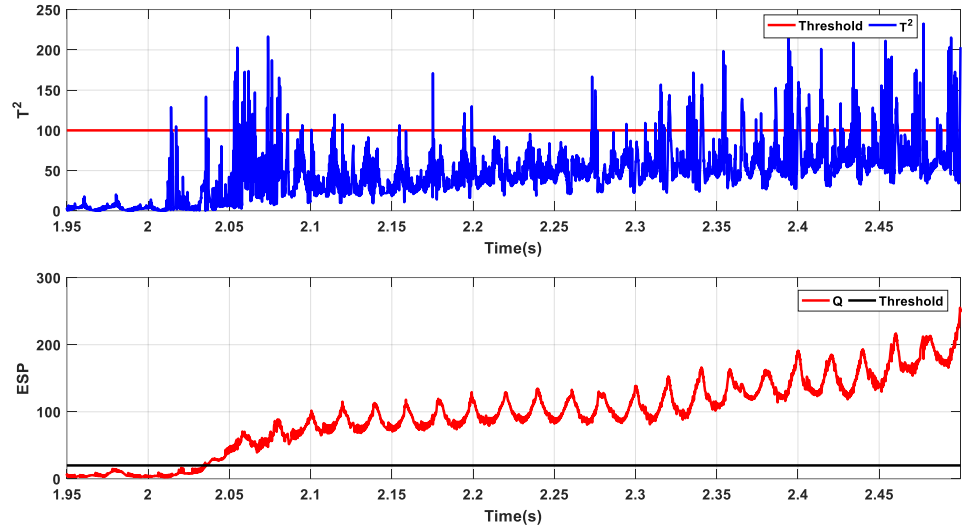


(a)

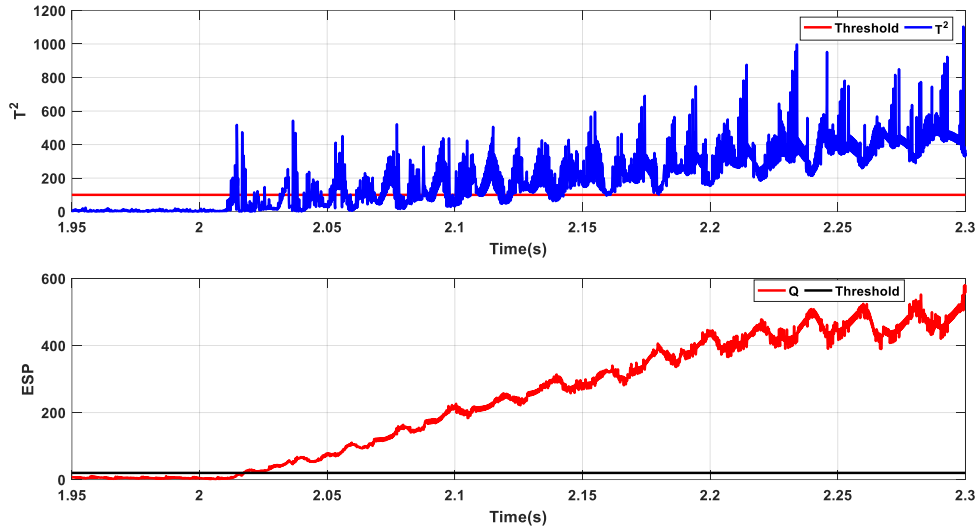


(b)

Figure 4.6: $T^2$ and $Q$ calculations using the same training set for the PCA and at different reference currents (a) $i_{ref}$=2A, (b) $i_{ref}$=4A

Similarly to the case of the MPC control, three eigenvalues can explain more than 95% of the data variation, as shown in Figure 4.7. Hence the new space in which the data is projected is composed of the three eigenvectors corresponding to the chosen three eigenvalues. The state variables considered in this case are the eight capacitor voltage along with the circulating and load currents. On the other hand, in the case of the voltage-balancing controller, the divergence of the two statistical tests is rather slow, and thus a trade-off between the threshold level and the fault detection speed is observed. As can be seen in Figure 4.8, for lower current values, the deviation of the $T^2$ and $Q$ is slower and thus, the detection time is increased. Consequently, the apriori knowledge about the working range (load variation) of the converter can help to establish proper threshold level. In fact, when considering the control of the MMC, the boundaries of the converter operations should be established in order to maintain the stability and the normal operation of the system.

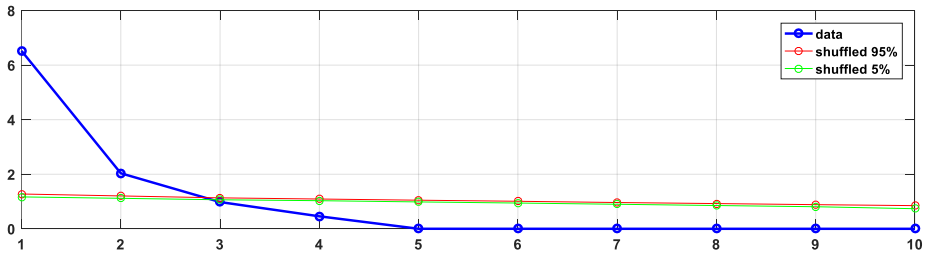


Figure 4.7: Eigenvalues of the ten state variables using voltage-balancing control and their importance

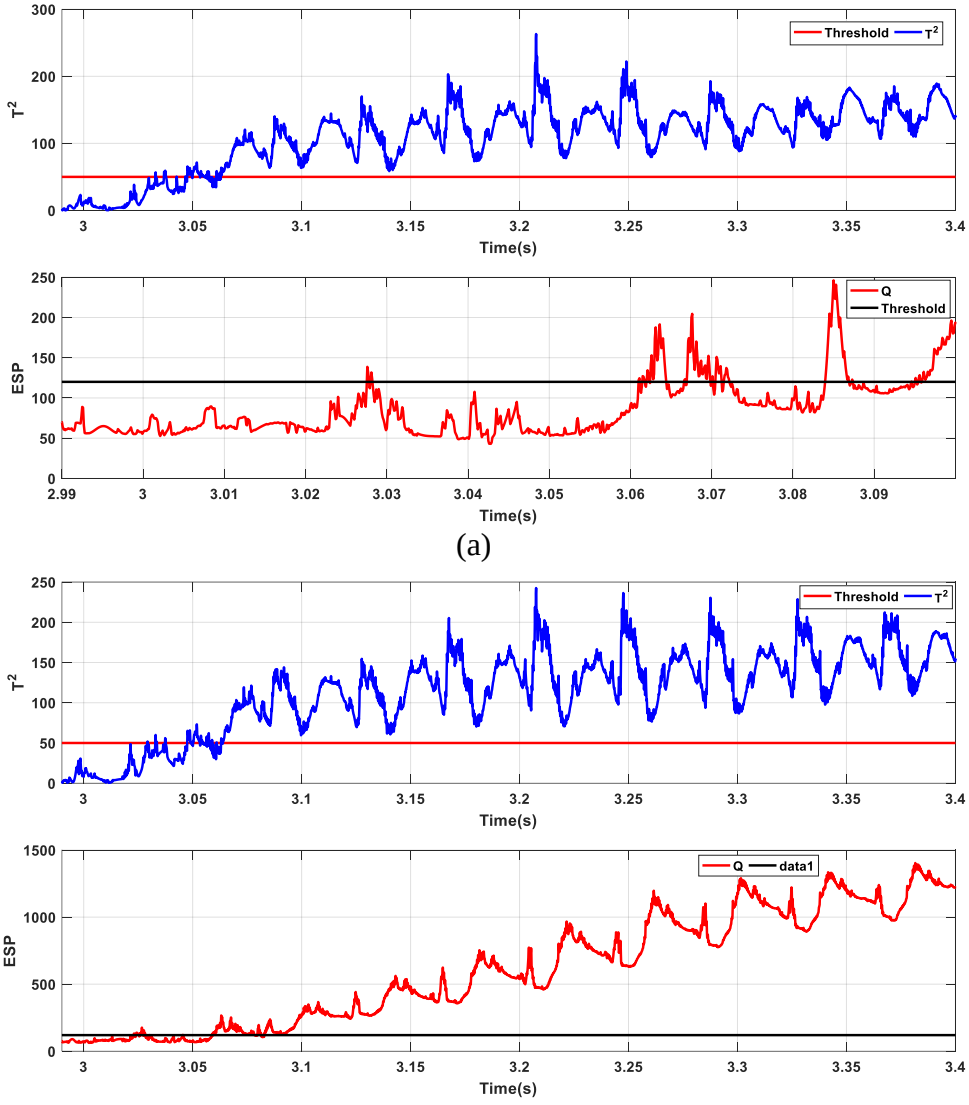


Figure 4.8: $T^2$ and $Q$ calculations using the same training set for the PCA and at different reference currents (a) $i_{load}$ =160A, (b) $i_{load}$=150A

### *4.3.2 Fault Detection using KPCA*

Similarly to the PCA case, the KPCA is capable of detecting faulty operating conditions. The KPCA algorithm is developed and tested under the same simulation conditions. However, the elaboration of the KPCA model is more complicated than the PCA model. An additional parameter, the kernel width $\sigma$ of the kernel matrix, has to be tuned to provide the best performance of the KPCA procedure. As the most popular function and due to its high calculation efficiency, the Radial Basis Function (RBF) is used as the kernel function. Similarly, the choice of the data reduction in the feature space is also challenging, since they should be appropriately chosen to guarantee the exploitation of the essential features of the data and neglect the disturbances that can affect the performance of the technique. The choice of the number of retained eigenvalues can be chosen using the following criteria

$$\frac{\sum \lambda_{retained}}{\sum \lambda_k} * 100 \geq \text{threshold} \qquad (4.1)$$

In this study, the threshold value is chosen equal to 99% based on 4-fold cross-validation, which allows good performance and noise reduction. In contrast, the choice of the kernel width is made through grid search and k-fold cross-validation. The grid search included values ranging from $2^{-12}$ up to $2^{12}$, and for each selected value 4-fold cross-validation is done. The best performance in the fault detection corresponds to $\sigma = 2^{-8}$.
The simulation results shown in Figure 4.9 depicts that the projection error using the KPCA procedure under MPC control can be an effective way to detect the novelties accurately in the converter with an acceptable detection time and also depending on the working conditions.

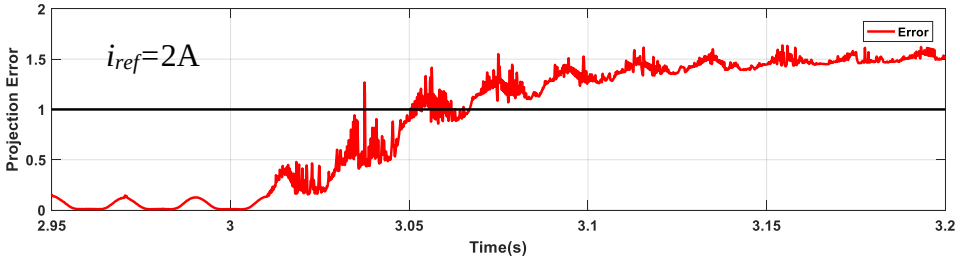


(a)

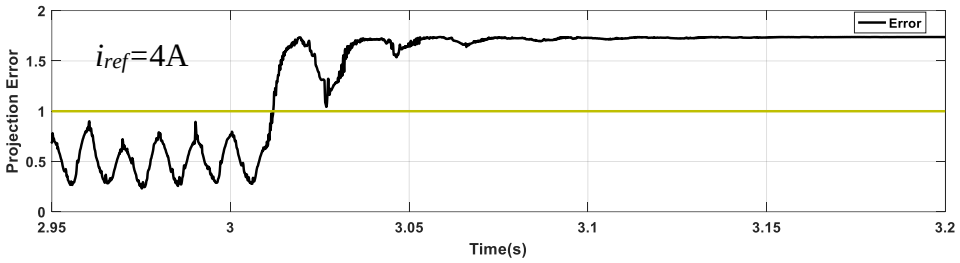


(b)

Figure 4.9: Projection error calculated using KPCA on the MPC controller and at different reference currents (a) $i_{ref}$ =2A, (b) $i_{ref}$=4A

The same remarks can be drawn in the KPCA case using the voltage-balancing control. The same threshold can be used to detect open circuit faults within a small range of current variation without loss of much detection time. As shown in Figure 4.10 (a) and (b), the load current varied from 160A to 150A, however, the variation in the detection time remained small (from 26*ms* to 27*ms*). Nevertheless, when the variation is significant (Figure 4.10 (c)), the detection time is affected, and the fault detection could only sense the

fault at $t_{fault}$=48$ms$.

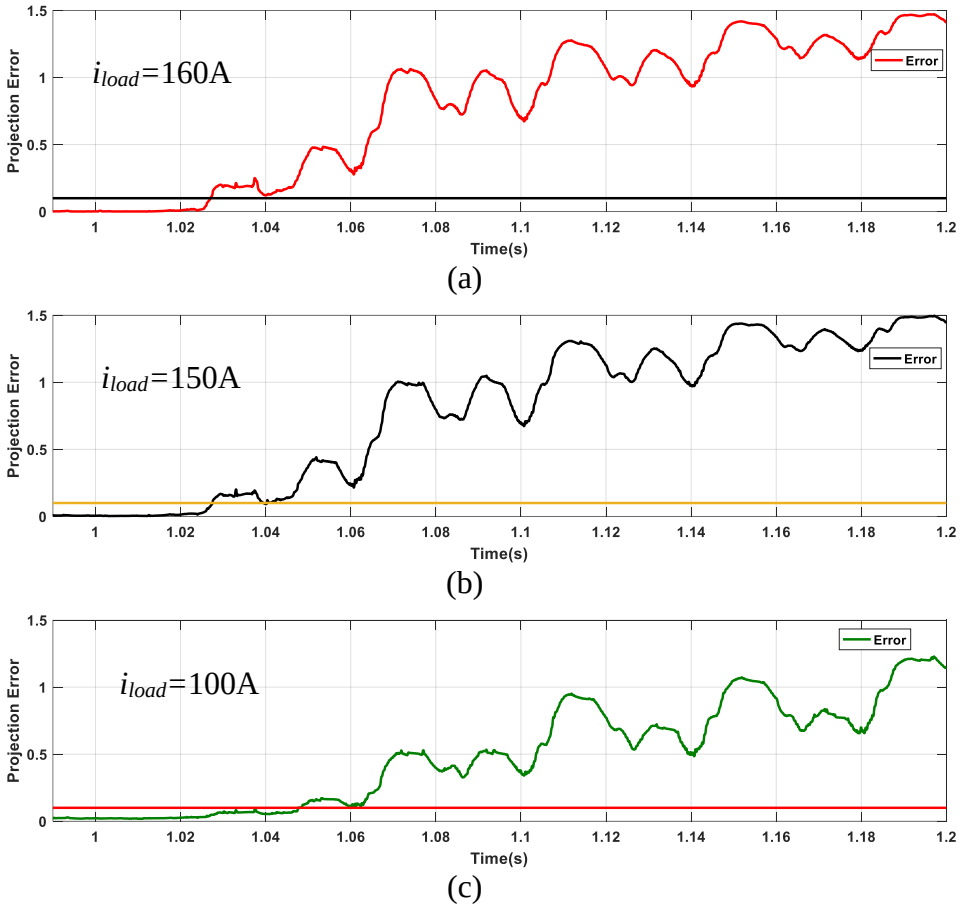


Figure 4.10: Projection error calculated using KPCA on the MPC controller and at different load currents (a) $i_{load}$ =160A, (b) $i_{load}$=150A, (c) $i_{load}$=100A

According to the observations regarding the choice of the best threshold that would allow false alarm free operations and fast fault detection time, the best option is to consider a range of thresholds that depends on the working conditions of the converter. This range can be built based on the apriori knowledge of the system load and its variations, and in a way that would cover the normal operations without false alarms and detect the faults in the needed time.

## 4.4 Open Circuit Fault Localization

The localization procedure is a crucial task in MMC, to keep the normal operations of the system. Usually, the fault detection procedure is followed by a fault tolerant control, which requires the exact location of the faulty cell in order to isolate it.

While the PCA is capable of accurately detecting the faults when they surge, the procedure is not capable of determining their locations. This is because this technique was designed to work with linear systems. The KPCA on the other hand, have excellent capabilities to deal with nonlinear systems. In this subsection, the fault localization using KPCA is discussed. The simulation results of fault localization presented in this subsection are the cumulative error over a period of 200*ms*, the capacitor voltages during this period and the instantaneous projection error.

### *4.4.1 Approach1: Full State Variables*

In this approach, the full states considered in the previous subsections (capacitor voltages, circulating and load currents) are used to perform the fault localization.

#### *4.4.1.1 Fault Localization under MPC Control*

The simulation parameters for both MPC and voltage-balancing control techniques are as depicted in subsections 4.1 and 4.2. The kernel parameter is chosen as $\sigma = 2^{-8,}$ and the training set is generated under load current $i_{load}$ =5A. As previously mentioned, the fault localization models are created using faulty data corresponding to each power switch. Thus, the resultant KPCA models are eight when the MPC with four cells is considered. The simulation results are shown in Figure 4.11 and Figure 4.12 using a load current of 4A and 2A, respectively, indicate that the procedure can effectively detect the faulty switch within the cell under load variation. The Figure 4.11 (a) represents the cumulative projection error in the feature space for each KPCA model designed (in this case there are eight KPCA models corresponding to eight susceptible faults), the line with the lowest cumulative error corresponds to the faulty cell (in this case the cumulative error corresponding to switch $T_1$ in cell $E_1$ has the lowest error, thus identified as the faulty switch). The Figure 4.11 (b) represents the corresponding capacitor voltage variations of each cell, and the Figure 4.11 (c) represents the instantaneous projection error, which is accumulated over time to provide the fault location. Note that the exact fault location is measured as the minimum cumulative error after fault detection by 200ms.

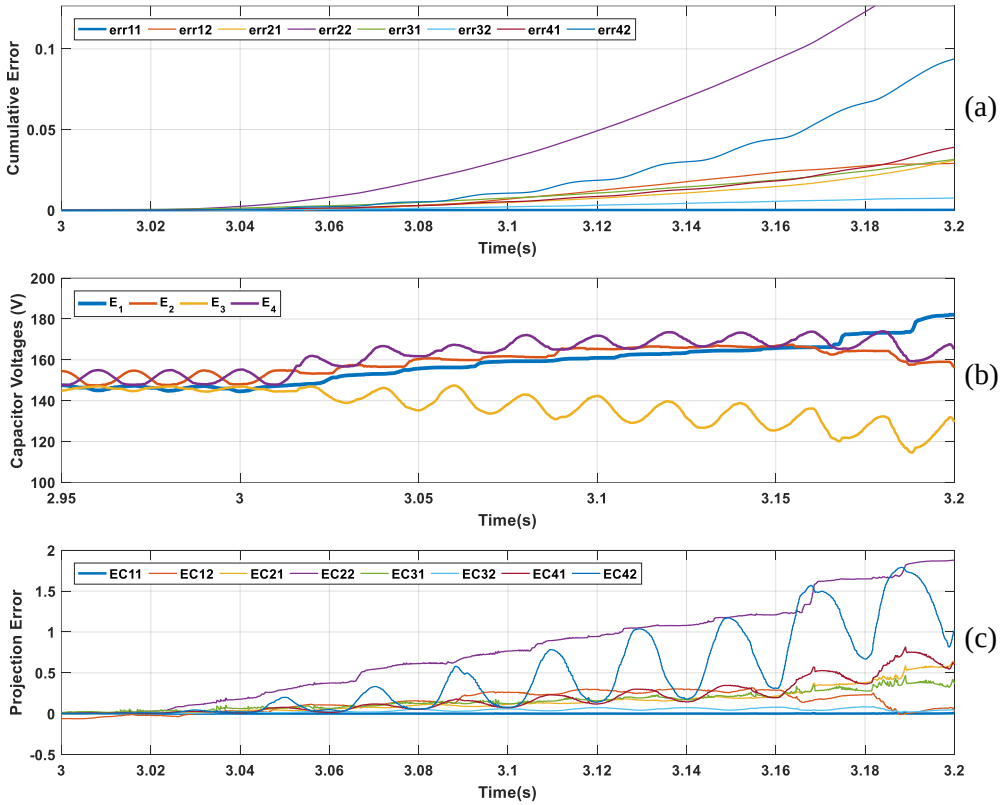


Figure 4.11: Fault localization results using MPC control when the fault occurred at $t$=3s in cell 1 switch $T_1$ and under load current $i_{load}$=4A

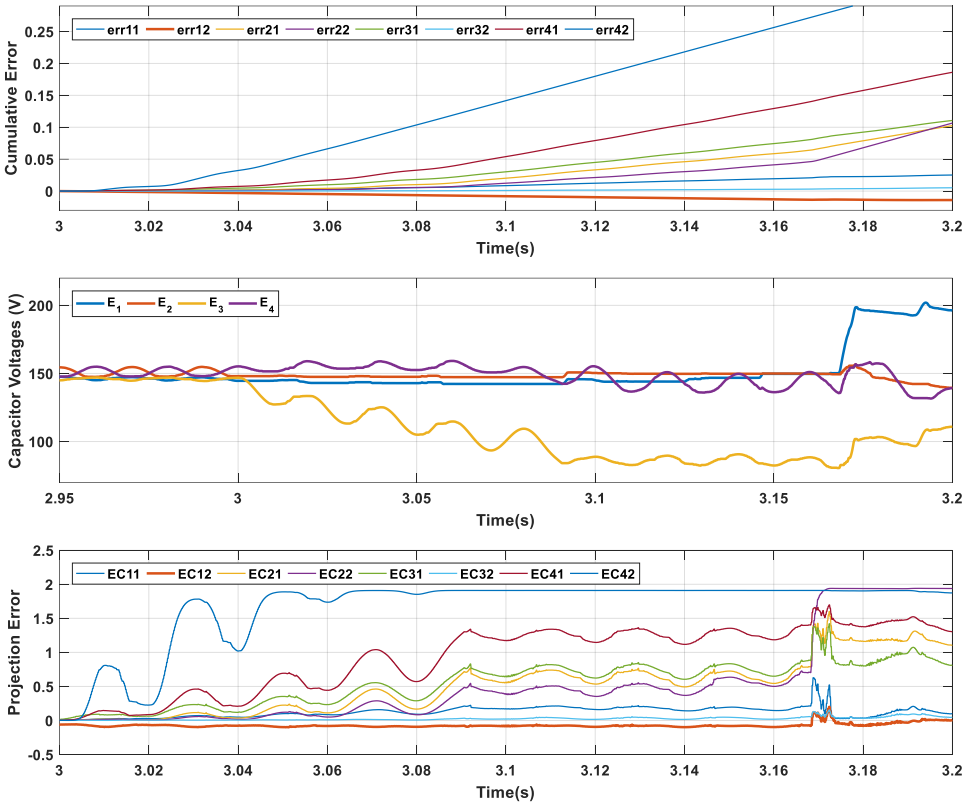


Figure 4.12: Fault localization results using MPC control when the fault occurred at $t$=3s in cell 1 switch $T_2$ and under load current $i_{load}$=2A

Similarly, Figure 4.13 shows that the fault localization procedure can effectively localize the faulty switch within the faulty cell. It can be noted that the capacitor voltage can take a long time to reach the same level that was reached in Figure 4.11, hence, the usage of a fixed threshold to monitor the capacitor voltage levels can show poor performance compared to the adopted KPCA technique.

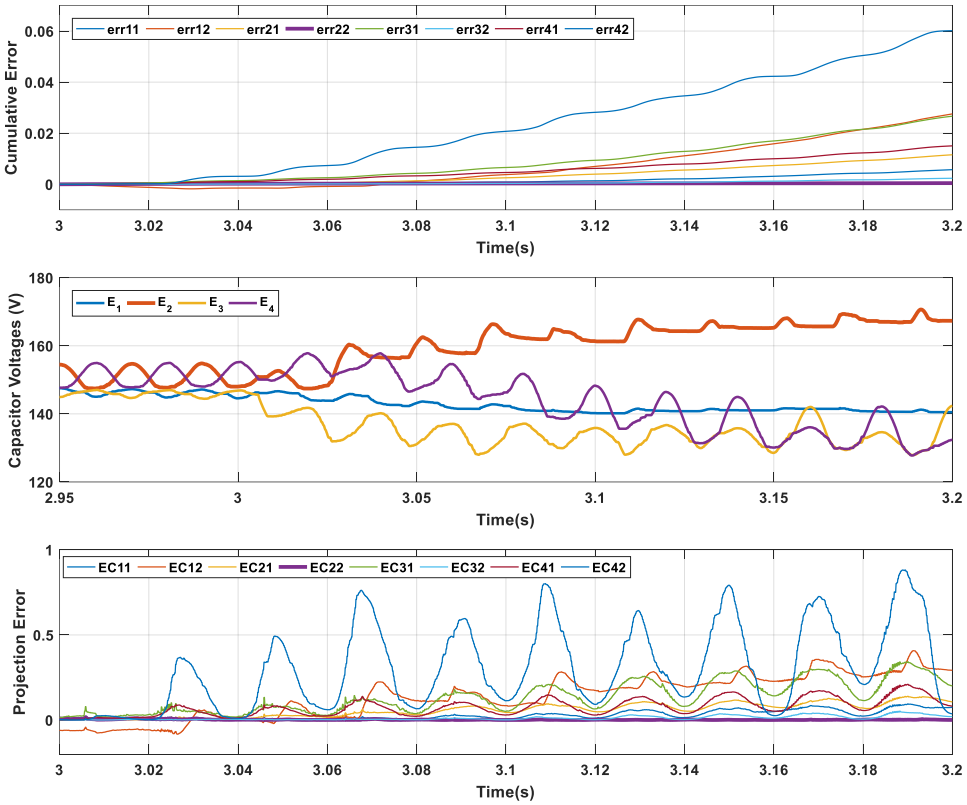


Figure 4.13: Fault localization results using MPC control when the fault occurred at $t$=3.005s in cell 2 switch $T_2$ and under load current $i_{load}$=3A

### *4.4.1.2 Fault Localization under voltage-balancing Control*

Similar to the MPC controller case, the KPCA with full state variables using a higher number of cells and a different control technique shows good performance in fault localization as depicted in Figure 4.14 and Figure 4.15. Note that the instantaneous and accumulated errors are much lower than the ones generated by the other KPCA models and

that the faulty switch can be identified in brief time.

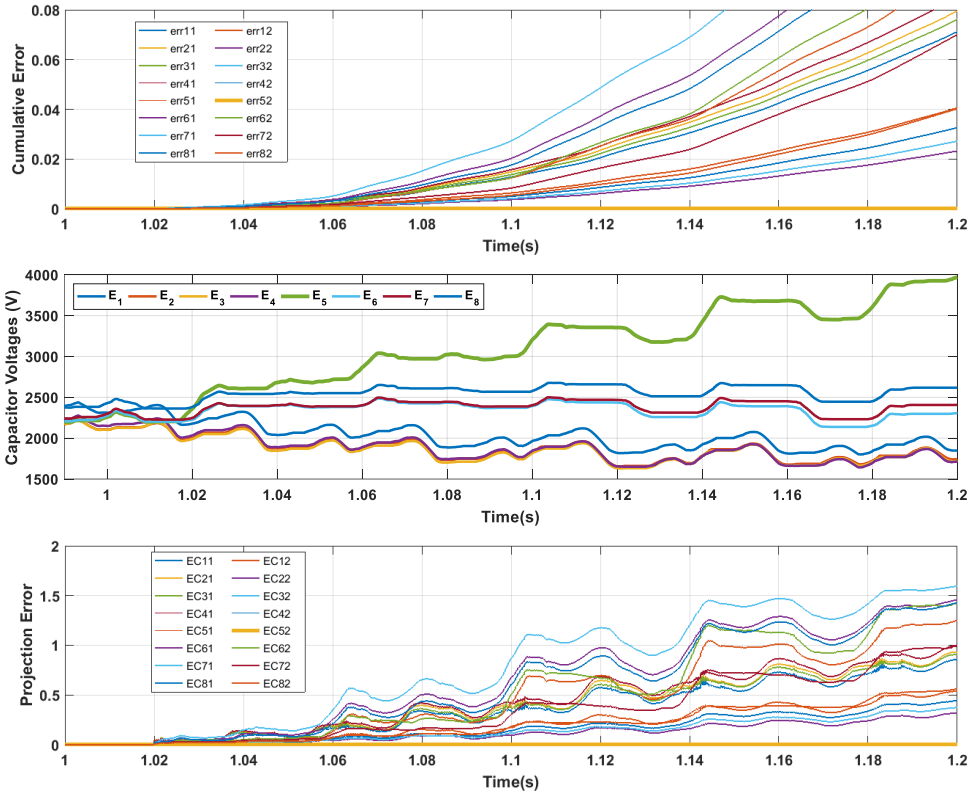


Figure 4.14: Fault localization results using voltage-balancing control when the fault occurred at $t$=1.01s in cell 5 switch $T_2$ and under load current $i_{load}$=150A

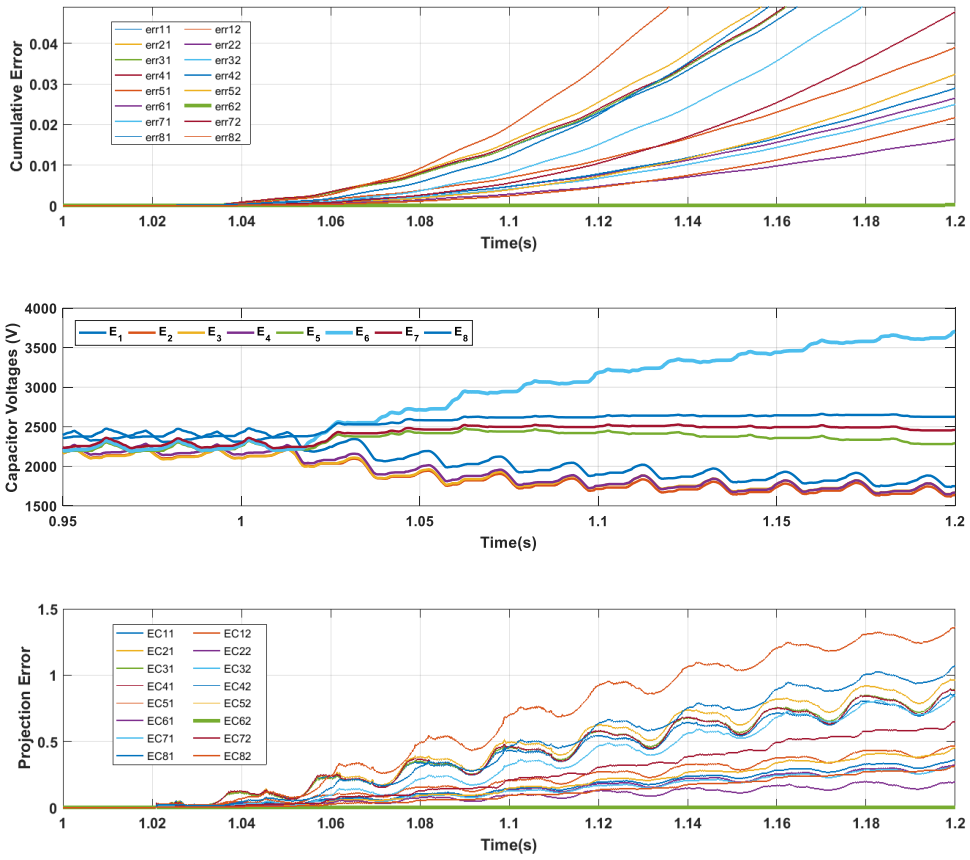


Figure 4.15: Fault localization results using voltage-balancing control when the fault occurred at $t$=1.015s in cell 6 switch $T_2$ and under load current $i_{load}$=160A

Numerous simulations have been conducted at different instants to evaluate the performance of the selected procedure. The simulated testing times correspond to different current levels, and directions, e.g., $t$ =1s correspond to arm current $i_{arm}$ =0, $t$ =1.005s correspond to the positive peak of the arm current, and $t$ =1.015s correspond to the negative peak. The current levels used to test the different approaches are $i_{load}$ = 2A and $i_{load}$ = 4A

for the MPC controller case and $i_{load}$ = 150A and $i_{load}$ = 160A for the voltage-balancing case. The fault localization procedure showed similar performance under the different current levels.

However, the procedure has misclassified some cells as shown in Figure 4.16. It can be seen that the variation of the capacitor voltage corresponding to the faulty cell is slow and, similarly, other capacitor voltages have raised above their normal values in the same rate which prevents the KPCA, in this case, to correctly identify the fault location. The misclassifications correspond to the case of upper switches open circuit faults. According to the Table 3.1, in case of upper switch open circuit fault, the cell is bypassed when the arm current is negative and the upper switch is inserted, whereas in case of lower switch open circuit fault, the cell capacitor charges when the arm current is positive regardless of the status of the switch (inserted or bypassed). From the aforementioned observations, the reason behind the misclassification of the faulty cells is due to the controller interference in case of upper switch faults since the controller can in some cases, when trying to balance the capacitor voltages, force the faulty cell to be bypassed when the current is negative, which result in slow variation of the state variables and requires longer time for localization in case full state raw variables are considered as input to the KPCA procedure. This behavior is not seen in the case of lower switches faults because the rate of capacitor voltage increase is independent of the gate signal.

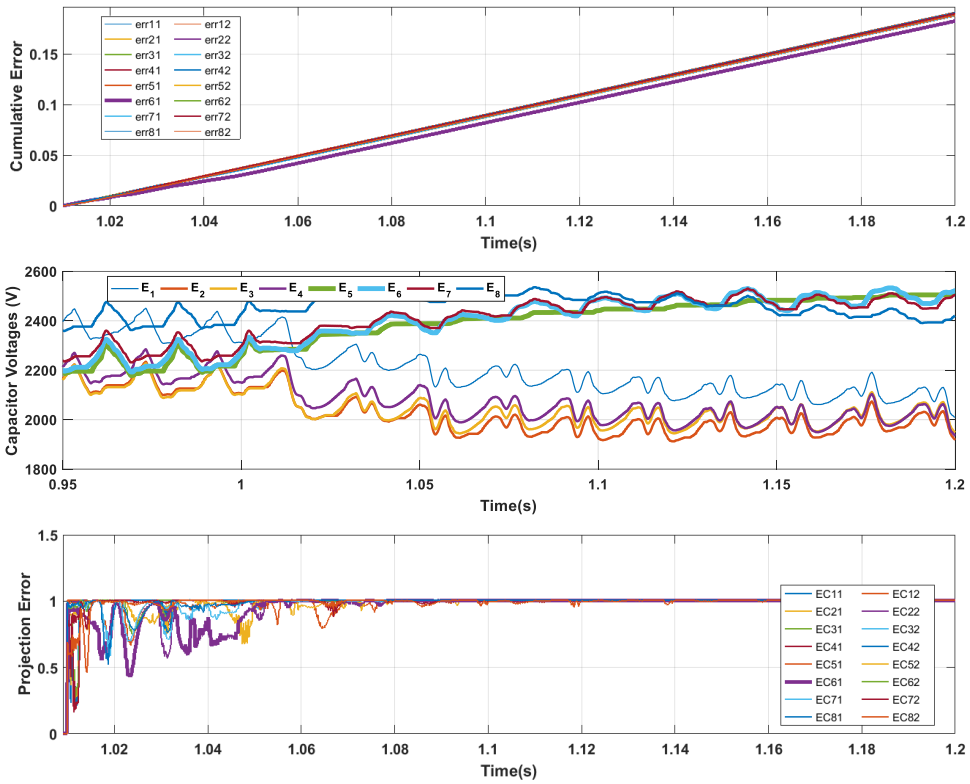


Figure 4.16: Fault localization results using voltage-balancing control when the fault occurred at $t$=1.015s in cell 6 switch $T_2$ and under load current $i_{load}$=150A

### *4.4.2 Approach2: Data Preprocessing with Capacitor Voltages as State Variables*

In contrast to the direct measurement and utilization of the data variables, data preprocessing can accentuate the discrepancy between the behaviors of different capacitor voltages under various faulty conditions. The capability to correctly localize the faulty cells can be increased by providing additional information that deems useful in differentiating the various states of the capacitor voltages. The fault impact alters the normal behavior of the system and impacts the sequence of the inserted and bypassed submodules generated

by the controller, which render some cases harder to identify. The involvement of the controller can be used to narrow the error location and as it can be seen from the different simulations, the controller tends to lower the capacitor voltages of the healthy arm in order to keep the balance between the two arms, which in consequence leads to the increase of the capacitor voltages of the faulty arm (the arm containing the faulty switch) since the total power received by the converter remained unchanged. Hence, the sum of the capacitor voltages of the faulty arm increases and the difference between the faulty and the healthy arm is always positive. Therefore, the attitude of the controller when the open circuit fault occurs provides a hint about the faulty arm. In contrast, the usage of the Euclidian distance, the cubic distance, and the normalization with regards of other capacitor voltages reduce the difference in behavior between the upper and lower switches of the faulty cell.

#### *4.4.2.1 Fault localization under MPC control*

In Figure 4.17, the simulation results of the fault localization using data preprocessing on a four cells converter using MPC controller at $t$= 3.02s under load current of 2A. It can be seen that the cumulative error corresponding to the faulty switch $E_4\ T_2$ is the lowest and the closest curve is the one corresponding to the upper switch of the same cell.

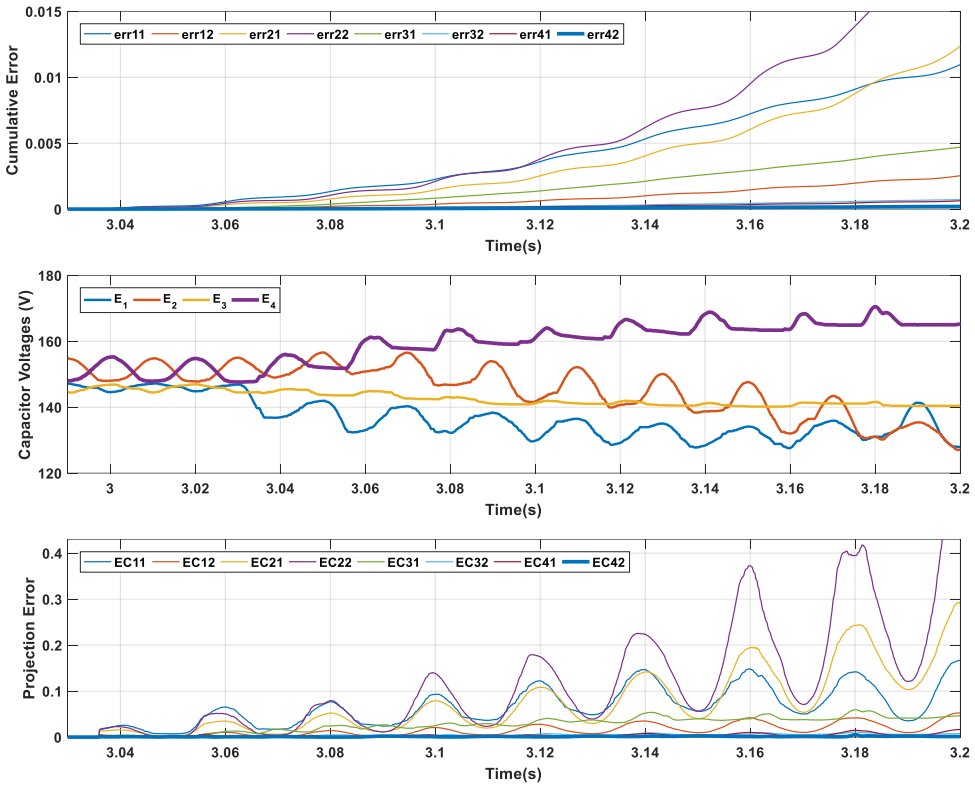


Figure 4.17: Fault localization results using MPC control when the fault occurred at $t$=3.02s in cell 4 switch $T_2$ and under load current $i_{load}$=2A

In Figure 4.18, an open circuit fault is injected in the upper switch $T_1$ of cell 3, at $t$=3.02s and the identified power switch is the lower switch of the same cell, which confirms the notes made earlier about misclassification within the same cell. This misclassification is acceptable in general, considering that the isolation procedure disengages or bypass the whole cell containing the faulty switch. The analysis of exact faulty switch can be done offline at a later stage when the cell is disconnected from the converter.

The success rate, in this case, is much higher that than the direct usage of full state variables case. All the simulations done using this technique achieved 100% accuracy in faulty cell localization but a lower accuracy if the exact faulty switch is considered.

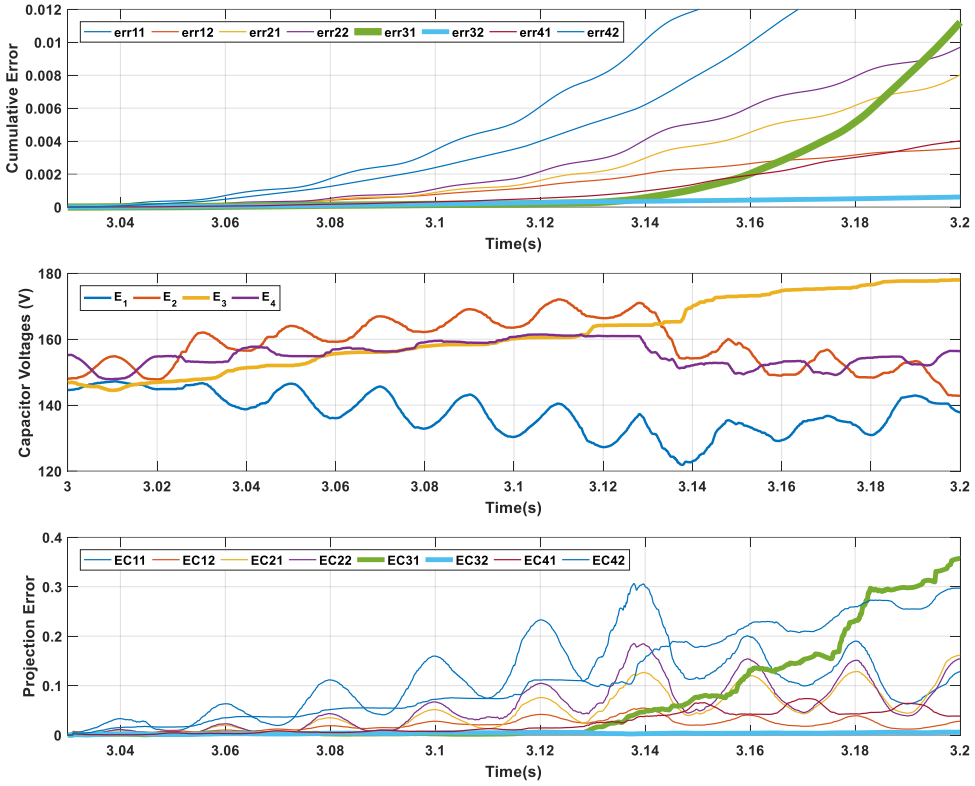


Figure 4.18: Fault localization results using MPC control when the fault occurred at $t$=3.02s in cell 3 switch $T_1$ and under load current $i_{load}$=2A

#### *4.4.2.2 Fault Localization under voltage-balancing Control*

To test the performance of the adopted technique, a converter with a higher number of cells (eight cells) and with different control scheme is used. The same accuracy (100%) is achieved when considering the faulty cell localization. In contrast, lower accuracy is obtained in faulty switch localization since the data preprocessing enlarges the discrepancy between the faulty cell and the other cells and, in contrast, it reduces the differences between the upper and lower cell switches within the faulty cell. Figure 4.19 showcases the simulation results of the KPCA using preprocessed data as input when an open circuit fault occurs in cell 8 switch $T_2$ at $t$=1.02s under load current $i_{load}$=160A. As it can be seen, the projection error corresponding to the faulty switch is much lower than the projection errors produced by the other healthy capacitor voltages.

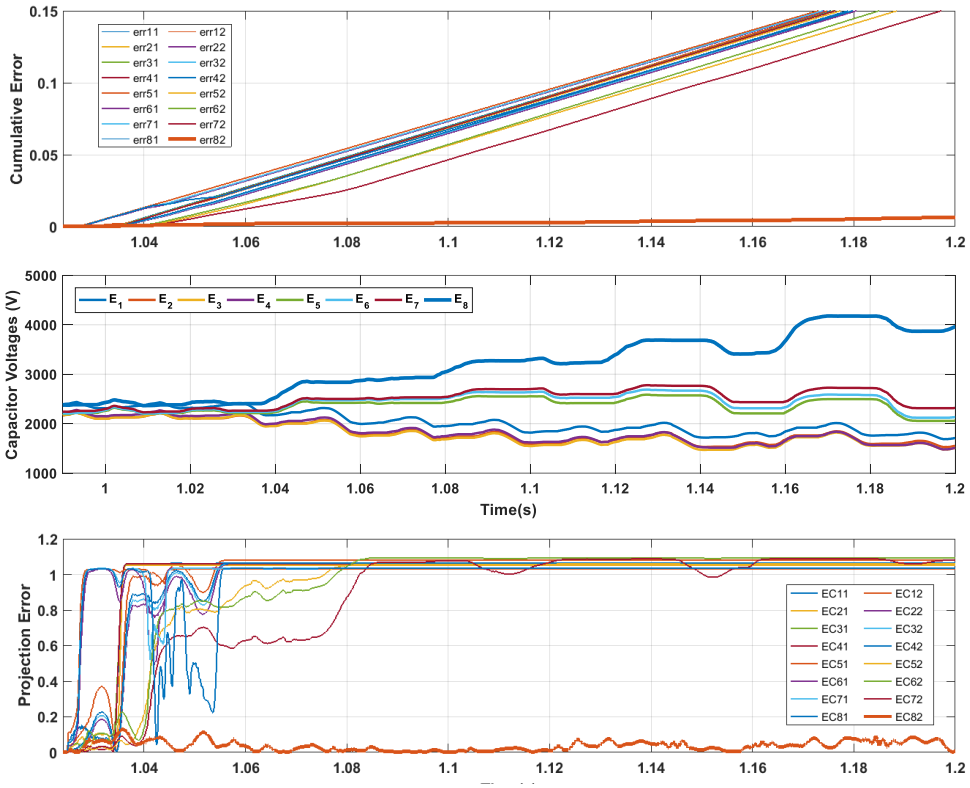


Figure 4.19: Fault localization results using voltage-balancing control when the fault occurred at $t$=1.02s in cell 8 switch $T_2$ and under load current $i_{load}$=160A

### *4.4.3 Approach3: Partial KPCA*

The partial KPCA (PKPCA) has a significant advantage over the two previous approaches, that is, the training phase is performed on the healthy data solely, that means there is no need to acquire the faulty data corresponding to each switch, which may deem hard to get. The PKPCA, on the other hand, can only verify the status of the cells, not the switches, which is acceptable considering what has been stated before; post localization procedure, the whole cell would be isolated. Simulation results of the PKPCA in the case

of voltage-balancing control are illustrated in Figure 4.20 and Figure 4.21. Although PKPCA managed to correctly locate most of the open circuit faults in case of voltage-balancing control, it failed to spot these faults in the case of MPC control and the success rate in identifying the faulty switch was low. Thus, it can be concluded that the PKPCA is not suitable for this type of control.

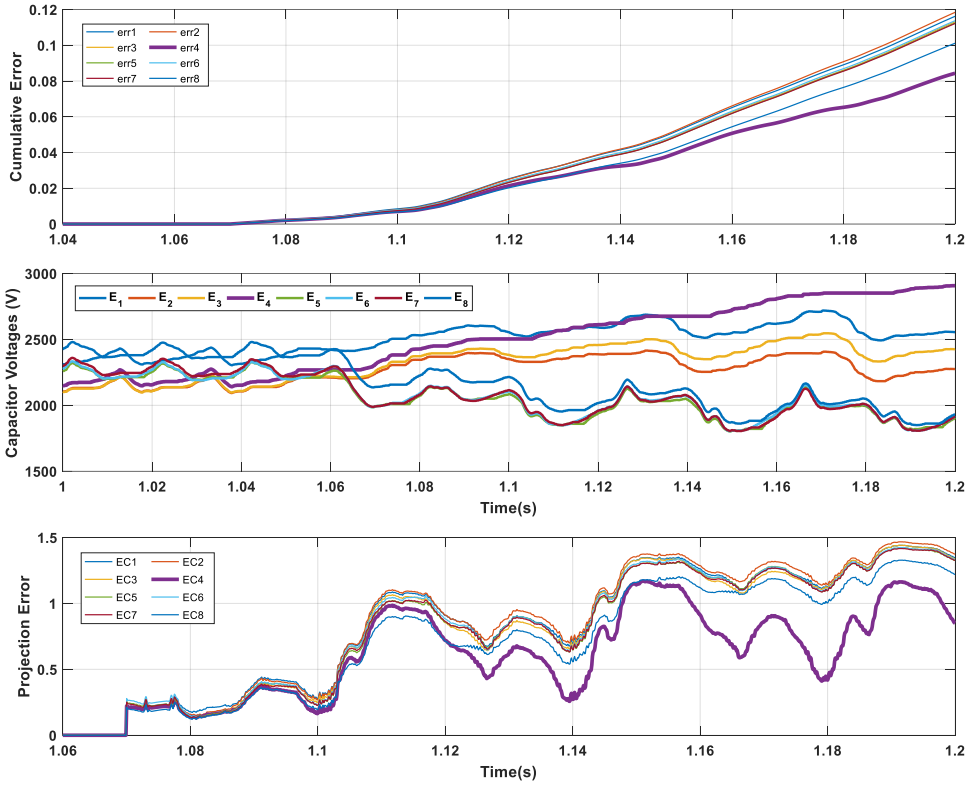


Figure 4.20: Fault localization results using voltage-balancing control when the fault occurred at $t$=1.005s in cell 4 switch $T_1$ and under load current $i_{load}$=150A

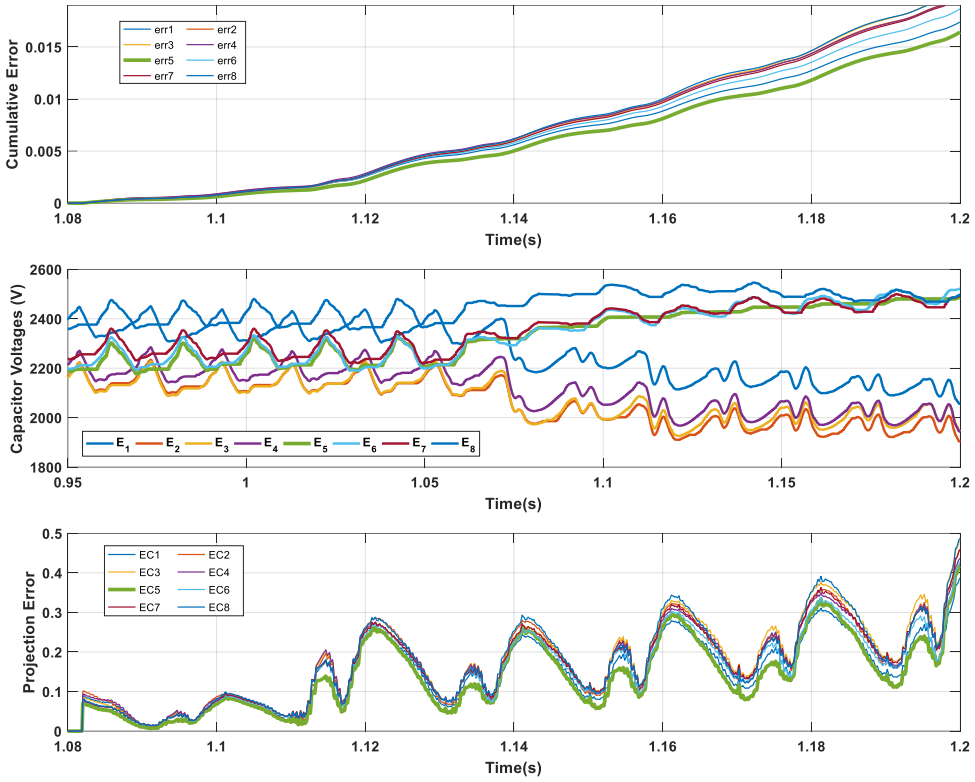


Figure 4.21: Fault localization results using voltage-balancing control when the fault occurred at $t$=1.05s in cell 5 switch $T_1$ and under load current $i_{load}$=160A

### *4.4.4 Performance Comparison*

To recapitulate the simulation results of the presented approaches, their overall performance, in terms of speed, complexity, computational time and effectiveness, should be compared. Table 4.3 illustrates the overall performance of the three approaches based on the aforementioned criteria. It should be noted that the terms Low, Medium and High are used to compare the performance of approaches between each other.

It may seem that the complexity to design the second approach is higher than the first one given that there will be a data preprocessing, but in fact, tuning the KPCA parameters in the first approach requires much more effort and time since a much smaller range of the kernel width $\sigma$ allow good performance. The complexity of the third approach is lower since the data used to train and test the KPCA is the data corresponding to the normal behavior of the system, which is always available even in practical work.

The computational time required by the second approach is higher than the both the first and the third approaches given the data preprocessing requirement. In contrast, the first approach works only on the cell level, which decreases the number of KPCA modules to half and thus requires much less time to execute.

Table 4.3: Performance comparison between the three adopted approaches of KPCA

| | Approach1 | Approach2 | Approach3 |
|---|---|---|---|
| Complexity | High | Medium | Low |
| Computational time | Medium | High | Low |
| Localization speed | High | High | High |
| Success rate (Cell level) | Medium | High | Low |

Although the design of the three approaches imposes the utilization of fixed localization time instead of the usage of a threshold, it is always good to quantify the performance of the presented approaches in terms of average and highest localization time

for both MMC configurations. Table 4.4, illustrate the localization performance of different approaches in terms of localization speed. It is clear that all the approaches have close localization speed in overall. However, the largest localization time recorded in case of voltage-balancing control is 200*ms* using, which is much higher than the average localization time. In fact, most of the faults were localized in brief time, which is an indication that the procedure is indeed capable of fast localization. On the other hand, the localization time of the third approach using MPC was rolled out of the calculations because of the low success rate in fault localization.

Table 4.4: Comparison of localization speed for the three approaches under two control configurations

| | | MPC | Voltage-Balancing |
|---|---|---|---|
| Approach1 | Average | 45*ms* | 25*ms* |
| | Highest | 140*ms* | 200*ms* |
| Approach2 | Average | 21*ms* | 35*ms* |
| | Highest | 88*ms* | 200*ms* |
| Approach3 | Average | NA | 41*ms* |
| | Highest | NA | 200*ms* |

The success rate is one of the most critical features that fault localization procedure has to offer since misclassifications lead to catastrophic results that can disrupt the normal operation of the whole system and can cause a total blackout. In this context, the performance of the three techniques is evaluated. As shown in Table 4.5, the accuracy of the localization procedure differs from one approach to the other. The most efficient approach is the second one that takes into account data preprocessing before performing the KPCA procedure. On the other hand, the lowest accuracy is associated with the third approach, which has a reasonable misclassification rate in the case of voltage-balancing control but the performance degrades drastically when the MPC control is deployed. One reason that can explain the low localization rate of the PKPCA is that the MPC controller has more significant interference with the fault behavior, which prevents the proper localization process. Besides, the training set of the two first approaches is a faulty set, which allows the KPCA to implicitly learn the converter behavior and thus, enhancing the localization performance.

Table 4.5: Cells localization accuracy of different approaches under two control topologies

| | MPC | Voltage-Balancing |
|---|---|---|
| Approach1 | 100% | 97.5% |
| Approach2 | 100% | 100% |
| Approach3 | 50% | 92.5% |

# CHAPTER 5: CONCLUSION AND FUTURE WORK

## 5.1 Conclusion

Modular Multilevel Converter is gaining significant interest in both industrial and scientific world. However, its specific structure and ability to address a significant amount of power require the integration of a considerable number of power switches, the most vulnerable component in multilevel converters. Therefore, to ensure the proper operation of the system, faults and abnormalities have to be detected and cleared at the earliest. This thesis has investigated the fault detection and localization of open circuit faults in power switches based on two multivariate statistical techniques, namely, the Principal Component Analysis and its nonlinear counterpart the Kernel Principal Component Analysis. The leverage of such techniques lies in the fact that they do not need the mathematical model of the system, that is, they are data-driven techniques. To ensure the optimum performance in fault detection, both procedures have to be trained on the normal operation of the converter, in order to extract the most valuable information and create a model that can separate the healthy and the faulty patterns. To test the performance of the adopted methodologies, two different control strategies are used along with two MMCs with different sizes and ratings. Both techniques showed high performance in detecting the abnormalities that alter the normal behavior of the converter. Nevertheless, working under a broad range of power rating may either render the detection slower or rise the probability of false alarms. However, the working boundaries of the converter are already known for proper operations of the converter and stability of the system, which allow the use of different thresholds for specific working ranges.

The advantages of PCA over its nonlinear counterpart is the simple formulation and the low computational effort in the monitoring phase along with a lower number of parameters to be tuned. Nevertheless, the KPCA strength lies in dealing with nonlinear systems. Therefore, while PCA failed to perform fault localization, three approaches were proposed using KPCA to overcome the limitations of PCA. The first approach considered the state variables of the system, namely, the capacitor voltages, and the circulating and load currents as inputs to the KPCA models, and the training is performed on the faulty data corresponding to each of the power switches. The second approach considered data preprocessing before proceeding to the KPCA models, in order to accentuate the discrepancy between the residuals of each model, which allow better localization performance. The third approach is the partial KPCA, which omits one state variable from the entry of each KPCA model and has the advantage to use the healthy data as the training set. The simulation results showed that data preprocessing enhances the classification procedure and tracks the fault back to its originating cell. However, this procedure revokes the difference between the behavior of the upper and lower switches of the faulty cell, which results in misclassifications within the same cell. Besides, this approach has the most considerable computational burden in comparison to the standard full state KPCA and the partial KPCA. On the other hand, partial KPCA had recorded a low success rate 50% and 92.5% for fault detection in MMC using MPC and voltage-balancing respectively, in comparison to 100% and 97.5% for the standard full state KPCA and 100% for both control techniques using data preprocessing. The localization time for all the approaches was similar that is less than or equal to 200*ms*. Hence, if an overall assessment can be made, one can conclude that if given the needed computational resources, the data preprocessing

before KPCA modeling is the best option for proper localization.

## 5.2 Future Work

The models presented in this thesis can be taken to the next step to explore more potentials under real situations. For instance, if a real system is considered, in the fault detection procedure, the relationship between the threshold and the working range can be neatly presented such that faults can be detected at an optimum time for both PCA and KPCA. Besides, considering other state variables as input to the standard KPCA can enhance its localization speed and accuracy especially that the KPCA does not depend on the size of input parameters but the number of samples considered. Similarly, finding more relationships between the input data in the preprocessing phase if the approach 2 for fault localization is considered, can reduce the localization time and avoid misclassifications within the faulty cell. Finally, upon fault occurrence, the controller tries to bring back the system to stability and thus affects the dynamics of the fault propagation, thus, finding a way to avoid the controller interference with the fault effect can enhance the overall performance of every data-driven localization procedure.

# REFERENCES


[1] L. M. Moore and H. N. Post, “Five Years of Operating Experience at a Large , Utility-scale Photovoltaic Generating Plant z,” no. December 2007, pp. 249–259, 2008.

[2] P. Tavner, “SUPERGEN Wind 2011 General Assembly,” *SUPERGEN Wind 2011 General Assembly*, no. March, 2011.

[3] H. Wang and M. Liserre, “Toward Reliable Power Electronics,” no. june, pp. 17–26, 2013.

[4] W. Energy, “Reliability of Different Wind Turbine Concepts with Relevance to Offshore Application,” no. April, 2008.

[5] S. Sheng and NREL, “Report on Wind Turbine Subsystem Reliability - A Survey of Various Databases,” *NREL/PR-5000-59111,National Renewable Energy Laboratory*, 2013.

[6] H. Wang and F. Blaabjerg, “Design for Reliability of Power Electronic Systems,” 2012.

[7] S. Yang *et al.*, “An Industry-Based Survey of Reliability in Power Electronic Converters,” vol. 47, no. 3, pp. 1441–1451, 2011.

[8] ZVEI, *Handbook for Robustness Validation of Automotive Electrical / Electronic Modules*. 2008.

[9] D. Miljković, “Fault Detection Methods: A Literature Survey,” *Proceedings of the 34th International Convention MIPRO*, pp. 750–755, 2011.

[10] S. Yang, D. Xiang, A. Bryant, P. Mawby, and S. Member, “Condition Monitoring

for Device Reliability in Power Electronic Converters : A Review," vol. 25, no. 11, pp. 2734–2752, 2010.

[11] V. K. Sundaramoorthy, E. Bianda, and G. J. Riedel, "A study to improve IGBT reliability in power electronics applications," *2015 International Semiconductor Conference (CAS)*, no. March, pp. 19–26, 2015.

[12] Z. Sarkany *et al.*, "Failure Prediction of IGBT Modules Based on Power Cycling Tests," vol. 2013, pp. 270–273, 2013.

[13] C. Busca, "Modeling Lifetime of High Power IGBTs in Wind Power Applications – An overview," pp. 1408–1413, 2011.

[14] M. Ciappa and W. Fichtner, "Lifetime Prediction of IGBT Modules for Traction Applications," pp. 0–6, 2000.

[15] R. Wu, F. Blaabjerg, H. Wang, M. Liserre, and F. Iannuzzo, "Catastrophic failure and fault-tolerant design of IGBT power electronic converters - An overview," in *IECON Proceedings (Industrial Electronics Conference)*, 2013, pp. 507–513.

[16] B. Lu, S. Member, and S. K. Sharma, "A Literature Review of IGBT Fault Diagnostic and Protection Methods for Power Inverters," *IEEE Transactions on Industry Applications*, vol. 45, no. 5, pp. 1770–1777, 2009.

[17] G. P. Adam, T. C. Lim, S. J. Finney, and B. W. Williams, "Voltage source converter in high voltage applications: multilevel versus two-level converters," *9th IET International Conference on AC and DC Power Transmission (ACDC 2010)*, pp. P03–P03, 2010.

[18] A. Lesnicar and R. Marquardt, "An innovative modular multilevel converter topology suitable for a wide power range," *2003 IEEE Bologna PowerTech* -

*Conference Proceedings*, vol. 3, pp. 272–277, 2003.

[19] G. P. Adam, O. Anaya-Lara, G. Burt, S. J. Finney, and B. W. Williams, "Comparison between flying capacitor and modular multilevel inverters," *2009 35th Annual Conference of IEEE Industrial Electronics*, pp. 271–276, 2009.

[20] S. Rohner, S. Bernet, M. Hiller, and R. Sommer, "Modulation, losses, and semiconductor requirements of modular multilevel converters," *IEEE Transactions on Industrial Electronics*, vol. 57, no. 8, pp. 2633–2642, 2010.

[21] S. Debnath, J. Qin, B. Bahrani, M. Saeedifard, and P. Barbosa, "Operation, Control, and Applications of the Modular Multilevel Converter: A Review," *IEEE Transactions on Power Electronics*, vol. PP, no. 99, pp. 1–1, 2014.

[22] S. P. Teeuwsen, "Modeling the trans bay cable project as voltage-sourced converter with modular multilevel converter design," *IEEE Power and Energy Society General Meeting*, pp. 1–8, 2011.

[23] S. Sau, S. Karmakar, and B. G. Fernandes, "Reduction of Capacitor Ripple Voltage and Current in Modular Multilevel Converter based Variable Speed Drives," *IECON 2017 - 43rd Annual conference of the IEEE*, pp. 1451–1456, 2017.

[24] Y. Chen, Z. Li, S. Zhao, X. Wei, and Y. Kang, "Design and Implementation of a Modular Multilevel Converter with Hierarchical Redundancy Ability for Electric Ship MVDC System," *IEEE Journal of Emerging and Selected Topics in Power Electronics*, vol. 5, no. 1, pp. 189–202, 2017.

[25] M. Vasiladiotis, A. Christe, T. Geyer, and A. Faulstich, "Decoupled Modulation Concept for Three-to-Single-Phase Direct AC / AC Modular Multilevel Converters for Railway Interties The decoupled modulation concept," pp. 1–9.

[26] L. Liu and N. Dai, “Hybrid railway power conditioner based on half-bridge modular multilevel converter,” *ECCE 2016 - IEEE Energy Conversion Congress and Exposition, Proceedings*, 2016.

[27] A. K. Sahoo, R. Otero-De-Leon, and N. Mohan, “Review of modular multilevel converters for teaching a graduate-level course of power electronics in power systems,” *45th North American Power Symposium, NAPS 2013*, 2013.

[28] S. Madichetty and A. Dasgupta, “Modular Multilevel Converters Part-I : A Review on Topologies , Modulation , Modeling and Control Schemes,” *International Journal of Power Electronics and Drive System (IJPEDS)*, vol. 4, no. 1, pp. 36–50, 2014.

[29] M. M. Harin, V. Vanitha, and M. Jayakumar, “Comparison of PWM Techniques for a three level Modular Multilevel Inverter,” *Energy Procedia*, vol. 117, pp. 666–673, 2017.

[30] A. Ghazanfari and Y. A. R. I. Mohamed, “A Resilient Framework for Fault-Tolerant Operation of Modular Multilevel Converters,” *IEEE Transactions on Industrial Electronics*, vol. 63, no. 5, pp. 2669–2678, 2016.

[31] V. Najmi, H. Nademi, and R. Burgos, “An Adaptive Backstepping Observer for Modular Multilevel Converter,” pp. 2115–2120, 2014.

[32] M. Rejas, L. Mathe, P. D. Burlacu, H. Pereira, M. Bongiorno, and R. Teodorescu, “Performance Comparison of Phase Shifted PWM and Sorting Method for Modular Multilevel Converters II Description of PSC-PWM technique and sorting algorithm Different strategies have been proposed in the literature to control the switches from,” *2015 17th European Conference on Power Electronics and Applications*

*(EPE'15 ECCE-Europe)*, no. Cd, pp. 1–10, 2015.

[33] M. Hagiwara and H. Akagi, "PWM control and experiment of modular multilevel converters," *Power Electronics Specialists Conference*, vol. 24, no. 7, pp. 154–161, 2008.

[34] B. J. Wei, "Review of Current Control Strategies in Modular Multilevel Converter," no. 4409124, 2016.

[35] A. Al-wedami, K. Al-hosani, and A. R. Beig, "Sliding Mode Observer of Submodular Capacitor Voltages in Modular Multilevel Converter," no. Mmc, 2015.

[36] G. P. Adam, O. Anaya-Lara, G. M. Burt, D. Telford, B. W. Williams, and J. R. McDonald, "Modular multilevel inverter: pulse width modulation and capacitor balancing technique," *IET Power Electronics*, vol. 3, no. 5, p. 702, 2010.

[37] F. Martinez-Rodrigo, D. Ramirez, A. Rey-Boue, S. de Pablo, and L. Herrero-de Lucas, "Modular Multilevel Converters: Control and Applications," *Energies*, vol. 10, no. 11, p. 1709, 2017.

[38] L. Ben-Brahim, A. Gastli, M. Trabelsi, K. A. Ghazi, M. Houchati, and H. Abu-Rub, "Modular Multilevel Converter Circulating Current Reduction Using Model Predictive Control," *IEEE Transactions on Industrial Electronics*, vol. 63, no. 6, pp. 3857–3866, 2016.

[39] S. Almasabi, N. Nguyen, and J. Mitra, "Control of a Multilevel Modular Converter using a state observer," *12th IEEE International Conference Electronics, Energy, Environment, Communication, Computer, Control: (E3-C3), INDICON 2015*, 2016.

[40] A. Lachichi and L. Harnefors, "Comparative analysis of control strategies for modular multilevel converters," *2011 IEEE Ninth International Conference on*

*Power Electronics and Drive Systems*, no. December, pp. 538–542, 2011.

[41] X. Zhang, J. Huang, Y. Sun, X. Tong, and Y. Rong, "Backstepping Controller for Modular Multilevel Converter," pp. 1–7.

[42] M. Abdelsalam, M. I. Marei, and S. B. Tennakoon, "An Integrated Control Strategy with Fault Detection and Tolerant Control Capability Based on Capacitor Voltage Estimation for Modular Multilevel Converters," *IEEE Transactions on Industry Applications*, vol. 53, no. 3, pp. 2840–2851, 2017.

[43] J. R. Lebre, R. F. Dias, and E. H. Watanabe, "POD-PWM applied to circulating current control in HVDC-MMC based system," *2015 IEEE 13th Brazilian Power Electronics Conference and 1st Southern Power Electronics Conference, COBEP/SPEC 2016*, 2015.

[44] J. Li, G. Konstantinou, H. R. Wickramasinghe, J. Pou, and X. Jin, "Offset PWM in Modular Multilevel Converters for Capacitor Voltage Reduction under Grid Imbalances," pp. 4538–4543, 2017.

[45] Y. Sun, C. A. Teixeira, D. G. Holmes, B. P. McGrath, and J. Zhao, "Low Order Circulating Current Suppression of PWM based Modular Multilevel Converters Using DC-link Voltage Compensation," *IEEE Transactions on Power Electronics*, vol. 33, no. 1, pp. 1–1, 2017.

[46] F. Simon, S. Fuchs, and S. Beck, "High Output Voltage Precision PWM for Modular Multilevel Converters."

[47] D. Li, Y. Sun, J. Zhao, and Z. Ji, "A Modified Voltage Measurement Technique for the Converters Using Module Grouping," pp. 589–594, 2017.

[48] P. I. R. U. Ulg, E. Sl, and D. F. Dh, "$q ,psuryhg 6sdfh 9hfwru 3:0 iru *ulg

&rqqhfwhg 00&," vol. 5, pp. 3–8.

[49] M. Saeedifard and R. Iravani, "Dynamic performance of a modular multilevel back-to-back HVDC system," *IEEE Transactions on Power Delivery*, vol. 25, no. 4, pp. 2903–2912, 2010.

[50] M. Winkelnkemper, A. Korn, and P. Steimer, "A modular direct converter for transformerless rail interties," *IEEE International Symposium on Industrial Electronics*, pp. 562–567, 2010.

[51] M. Salehifar, R. S. Arashloo, M. Moreno-Eguilaz, V. Sala, and L. Romeral, "A simple and robust method for open switch fault detection in power converters," *2013 9th IEEE International Symposium on Diagnostics for Electric Machines, Power Electronics and Drives (SDEMPED)*, pp. 461–468, 2013.

[52] A. Yazdani, H. Sepahvand, M. L. Crow, and M. Ferdowsi, "Fault Detection and Mitigation in Multilevel Converter STATCOMs," *IEEE Transactions on Industrial Electronics*, vol. 58, no. 4, pp. 1307–1315, 2011.

[53] S. Sedghi, A. Dastfan, and A. Ahmadyfard, "Fault detection and reconfiguration of a modular multilevel inverter using histogram analysis and neural network," *International Review on Modelling and Simulations*, vol. 4, no. 5, pp. 2057–2065, 2011.

[54] M. Alavi, D. Wang, and M. Luo, "Short-circuit fault diagnosis for three-phase inverters based on voltage-space patterns," *IEEE Transactions on Industrial Electronics*, vol. 61, no. 10, pp. 5558–5569, 2014.

[55] G. T. Son *et al.*, "Design and control of a modular multilevel HVDC converter with redundant power modules for noninterruptible energy transfer," *IEEE Transactions*

*on Power Delivery*, vol. 27, no. 3, pp. 1611–1619, 2012.

[56] R. Picas, S. Member, J. Zaragoza, J. Pou, S. Member, and S. Ceballos, "Reliable Modular Multilevel Converter Fault Detection with Redundant Voltage Sensor," vol. 8993, no. c, pp. 1–13, 2016.

[57] Q. Yang, J. Qin, and M. Saeedifard, "SubModule Failure Detection Methods for the Modular Multilevel Converter," pp. 3331–3337, 2015.

[58] S. Shao, A. J. Watson, J. C. Clare, S. Member, P. W. Wheeler, and S. Member, "Robustness Analysis and Experimental Validation of a Fault Detection and Isolation Method for the Modular Multilevel Converter," vol. 31, no. 5, pp. 3794–3805, 2016.

[59] H. Liu, P. C. Loh, F. Blaabjerg, L. Hui, L. Poh Chiang, and F. Blaabjerg, "Review of fault diagnosis and fault-tolerant control for modular multilevel converter of HVDC," *Industrial Electronics Society, IECON 2013 - 39th Annual Conference of the IEEE*, pp. 1242–1247, 2013.

[60] R. Picas, S. Member, J. Zaragoza, J. Pou, S. Member, and S. Ceballos, "Reliable Modular Multilevel Converter Fault Detection With Redundant Voltage Sensor," vol. 32, no. 1, pp. 39–51, 2017.

[61] H. Salimian, H. Iman-eini, and S. Farhangi, "Open-Circuit Fault Detection and Localization in Modular Multilevel Converter," no. February, pp. 3–4, 2015.

[62] X. Hu, J. Zhang, S. Xu, and Y. Jiang, "Fault Diagnosis of Modular Multilevel Converters Based on Extended State Observer," vol. 0, no. c, 2016.

[63] B. Li, S. Shi, B. Wang, G. Wang, W. Wang, and D. Xu, "Fault diagnosis and tolerant control of single IGBT open-circuit failure in modular multilevel converters," *IEEE*

*Transactions on Power Electronics*, vol. 31, no. 4, pp. 3165–3176, 2016.

[64] S. Shao, P. W. Wheeler, J. C. Clare, and A. J. Watson, "Fault Detection for Modular Multilevel Converters Based on Sliding Mode Observer," vol. 28, no. 11, pp. 4867–4872, 2013.

[65] K. Li, Z. Zhao, L. Yuan, S. Lu, and Y. Jiang, "Fault detection and tolerant control of open-circuit failure in MMC with full-bridge sub-modules," *ECCE 2016 - IEEE Energy Conversion Congress and Exposition, Proceedings*, 2016.

[66] F. Deng, Z. Chen, S. Member, and M. R. Khan, "Fault Detection and Localization Method for Modular Multilevel Converters," vol. 30, no. 5, pp. 2721–2732, 2015.

[67] S. Haghnazari, M. Khodabandeh, and M. R. Zolghadri, "Fast fault detection method for modular multilevel converter semiconductor power switches," pp. 165–174, 2015.

[68] X. Hu, J. Zhang, S. Xu, and J. Hang, "Extended State Observer based Fault Detection and Location Method for Modular Mu l tilevel Converters," pp. 0–5, 2016.

[69] S. Shao, J. C. Clare, A. J. Watson, and P. W. Wheeler, "Detection and isolation of multiple faults in a modular multilevel converter based on a sliding mode observer," *2014 IEEE Energy Conversion Congress and Exposition (ECCE)*, no. 3, pp. 3491–3495, 2014.

[70] Q. Yang, J. Qin, and M. Saeedifard, "Analysis, Detection, and Location of Open-Switch Submodule Failures in a Modular Multilevel Converter," *IEEE Transactions on Power Delivery*, vol. 31, no. 1, pp. 155–164, 2016.

[71] M. Abdelsalam, S. B. Tennakoon, A. L. Griffiths, and M. I. Marei, "A smart fault

detection and localization strategy of modular multi-level converters for HVDC networks," *IET Conference Publications*, vol. 2016, no. CP694, pp. 1–6, 2016.

[72] S. Haghnazari, M. Shahbazi, and M. R. Zolghadri, "A new fault detection method for modular multilevel converter semiconductor power switches," in *IECON 2015 - 41st Annual Conference of the IEEE Industrial Electronics Society*, 2015, pp. 50–55.

[73] S. Haghnazari and M. Shahbazi, "A New Fault Detection Method for Modular Multilevel Converter Semiconductor Power Switches," pp. 50–55, 2015.

[74] S. Shao, P. W. Wheeler, J. C. Clare, and A. J. Watson, "Open-circuit fault detection and isolation for modular multilevel converter based on sliding mode observer," *2013 15th European Conference on Power Electronics and Applications (EPE)*, pp. 1–9, 2013.

[75] D. Zhou, S. Yang, and Y. Tang, "A Voltage-Based Open-Circuit Fault Detection and Isolation Approach for Modular Multilevel Converters with Model Predictive Control," *IEEE Transactions on Power Electronics*, vol. 8993, no. c, pp. 1–9, 2018.

[76] M. M. Abdallah, "Fault Detection and Isolation of MMC under Submodule Open Circuit Fault," no. December, pp. 19–21, 2017.

[77] M. Abdelsalam, H. Diab, S. Tennakoon, A. Griffiths, and M. I. Marei, "Detection and diagnosis of sub-module faults for modular multilevel converters," in *2016 51st International Universities Power Engineering Conference (UPEC)*, 2016, pp. 1–6.

[78] S. Yang, Y. Tang, and P. Wang, "Open-circuit fault diagnosis of switching devices in a modular multilevel converter with distributed control," in *2017 IEEE Energy Conversion Congress and Exposition (ECCE)*, 2017, pp. 4208–4214.

[79] K. Xu, S. Xie, Y. Yan, Z. Zhang, B. Zhang, and Q. Qian, “Fault detection method for IGBT open-circuit faults in the modular multilevel converter based on predictive model,” in *2017 IEEE Energy Conversion Congress and Exposition (ECCE)*, 2017, no. 2, pp. 4190–4195.

[80] J. Wang, H. Ma, and Z. Bai, “A Submodule Fault Ride-Through Strategy for Modular Multilevel Converters with Nearest Level Modulation,” *IEEE Transactions on Power Electronics*, vol. 33, no. 2, pp. 1597–1608, 2018.

[81] D. Garcia, “Fault detection using Principal Component Analysis (PCA) in a wastewater treatment plant (WWTP),” 2009.

[82] T. Villegas, M. J. Fuente, and M. Rodríguez, “Principal component analysis for fault detection and diagnosis. experience with a pilot plant,” *Proceedings of the 9th WSEAS International conference on computational intelligence, man-machine systems and cybernetics*, pp. 147–152, 2010.

[83] G. R. Halligan and S. Jagannathan, “PCA-based fault isolation and prognosis with application to pump,” *International Journal of Advanced Manufacturing Technology*, vol. 55, no. 5–8, pp. 699–707, 2011.

[84] S. M. Holland, “Principal components analysis.,” *Methods in molecular biology (Clifton, N.J.)*, vol. 930, no. May, pp. 527–47, 2013.

[85] H. Abdi and L. J. Williams, “Principal component analysis,” *Wiley Interdisciplinary Reviews: Computational Statistics*, vol. 2, no. 4, pp. 433–459, 2010.

[86] D. Mining, “Principal Components : Mathematics , Example , Interpretation,” no. September, 2009.

[87] M. Ahmed, M. Baqqar, F. Gu, and A. D. Ball, “Fault detection and diagnosis using

Principal Component Analysis of vibration data from a reciprocating compressor," *Proceedings of the 2012 UKACC International Conference on Control, CONTROL 2012*, no. September, pp. 461–466, 2012.

[88] A. Alkaya and I. Eker, "Wavelet - Based principal component analysis for process monitoring with experimental application," *International Conference on Electrical and Electronics Engineering*, pp. 634–638, 2013.

[89] B. Schölkopf, A. Smola, and K.-R. Müller, "Nonlinear Component Analysis as a Kernel Eigenvalue Problem," *Neural Computation*, vol. 10, no. 5, pp. 1299–1319, 1998.

[90] M. Navi, M. R. Davoodi, and N. Meskin, "Sensor fault detection and isolation of an industrial gas turbine using partial kernel PCA," *IFAC-PapersOnLine*, vol. 28, no. 21, pp. 1389–1396, 2015.

[91] B. Scholkopf, a J. Smola, and K. R. Muller, "Kernel Principal Component Analysis," *Computer Vision And Mathematical Methods In Medical And Biomedical Image Analysis*, vol. 1327, pp. 583–588, 2012.

[92] M. H. Nguyen and F. De Torre, "Robust Kernel Principal Component Analysis," pp. 1–8.

[93] M. Z. Sheriff, M. N. Karim, M. N. Nounou, H. Nounou, and M. Mansouri, "Fault detection of nonlinear systems using an improved KPCA method," *2017 4th International Conference on Control, Decision and Information Technologies (CoDIT)*, pp. 0036–0041, 2017.

[94] J. M. Lee, C. K. Yoo, and I. B. Lee, "Fault detection of batch processes using multiway kernel principal component analysis," *Computers and Chemical*

*Engineering*, vol. 28, no. 9, pp. 1837–1847, 2004.

[95] S. W. Choi, C. Lee, J. M. Lee, J. H. Park, and I. B. Lee, "Fault detection and identification of nonlinear processes based on kernel PCA," *Chemometrics and Intelligent Laboratory Systems*, vol. 75, no. 1, pp. 55–67, 2005.

[96] R. Osadchy, "Kernel PCA - Unsupervised Learning 2011," 2011.

[97] J. M. Lee, S. J. Qin, and I. B. Lee, "Fault Detection of Non-Linear Processes Using Kernel Independent Component Analysis," *The Canadian Journal of Chemical Engineering*, vol. 85, no. 4, pp. 526–536, 2007.

[98] V. H. Nguyen and J. C. Golinval, "Fault detection based on Kernel Principal Component Analysis," *Engineering Structures*, vol. 32, no. 11, pp. 3683–3691, 2010.

[99] P. Cui, J. Li, and G. Wang, "Improved kernel principal component analysis for fault detection," *Expert Systems with Applications*, vol. 34, no. 2, pp. 1210–1219, 2008.

[100] M. A. Bin Shams, "Fault Identification using Kernel Principle Component Analysis," *The 18th IFAC World Congress*, pp. 4320–4325, 2011.

[101] M. Navi, M. Davoodi, and N. Meskin, "Sensor Fault Detection and Isolation of an Autonomous Underwater Vehicle Using Partial Kernel PCA," in *IEEE Conference on Prognostics and Health Management (PHM)*, 2015, pp. 1–9.

[102] A. Nowicki, M. Grochowski, and K. Duzinkiewicz, "Data-driven models for fault detection using kernel PCA: A water distribution system case study," *International Journal of Applied Mathematics and Computer Science*, vol. 22, no. 4, pp. 939–949, 2012.